Ore Geology Reviews 75 (2016) 220–238

Contents lists available at ScienceDirect

Ore Geology Reviews

journal homepage: www.elsevier.com/locate/oregeorev

Geochemistry of platinum-group elements and mineral composition in chromitites and associated rocks from the Abdasht ultramafic complex, Kerman, Southeastern Iran

Ali Reza Najafzadeh [a,*], Hamid Ahmadipour [b]

[a] Department of Geology, Payame Noor University, PO Box 19395-3697, Tehran, Iran
[b] Department of Geology, Faculty of Science, Shahid Bahonar University, Kerman, Iran

ARTICLE INFO

Article history:
Received 4 October 2015
Received in revised form 15 December 2015
Accepted 21 December 2015
Available online 31 December 2015

Keywords:
Abdasht ultramafic complex
Iran
Platinum-group elements
Podiform chromitites
Supra-subduction zone

ABSTRACT

The Abdasht complex is a major ultramafic complex in south-east Iran (Esfandagheh area). It is composed mainly of dunite, harzburgite, podiform chromitites, and subordinate lherzolite and wehrlite. The podiform chromitites display massive, disseminated, banded and nodular textures. Chromian spinels in massive chromitites exhibit a uniform and restricted composition and are characterized by Cr# [= Cr / (Cr + Al)] ranging from 0.76 to 0.77, Mg# [= Mg/(Mg + Fe^{2+})] from 0.63 to 0.65 and TiO_2 < 0.2 wt.%. These values may reflect crystallization of the chromian spinels from boninitic magmas. Chromian spinels in peridotites exhibit a wide range of Cr# from 0.48 to 0.86, Mg# from 0.26 to 0.56 and very low TiO_2 contents (averaging 0.07 wt.%). The Fe^{3+}# is very low, (<0.08 wt.%) in the chromian spinel of chromitites and peridotites of the Abdasht complex which reflects crystallization under low oxygen fugacities.

The distribution of platinum group elements (PGE) in Abdasht chromitites displays a high (Os + Ir + Ru)/(Rh + Pt + Pd) ratio with strongly fractionated chondrite-normalized PGE patterns typical of ophiolitic chromitites. Moreover, the Pd/Ir value, which is an indicator of PGE fractionation, is very low (<0.1) in the chromitites.

The harzburgite, dunite and lherzolite samples are highly depleted in PGE contents relative to chondrites. The Pd_N/Ir_N ratios in dunites are unfractionated, averaging 0.72, whereas the harzburgites and lherzolites show slightly positive slopes PGE spidergrams, together with a small positive Ru anomaly, and their Pd_N/Ir_N ratio averages 2.4 and 2.3 respectively. Moreover, the PGE chondrite and primitive mantle normalized patterns of harzburgite, dunite and lherzolite are relatively flat which are comparable to the highly depleted mantle peridotites.

The mineral chemistry data and PGE geochemistry indicate that the Abdasht chromitites and peridotites were generated from a melt with boninitic affinity under low oxygen fugacity in a supra-subduction zone setting. The composition of calculated parental melts of the Abdasht chromitites is consistent with the differentiation of arc-related magmas.

1. Introduction

Mafic-ultramafic complexes occur in various tectonic settings and information about their petrogenesis informs models of tectonics and crustal evolution (e.g. Su et al., 2011; Thanh et al., 2014). Moreover, ultramafic complexes from different tectonic settings provide information about the paleogeodynamic history and crustal evolution in continental and oceanic regions (e.g. Ghosh et al., 2013).

Chromian spinel is well established alteration-resistant petrogenetic indicator of the tectonic setting of ultramafic–mafic complexes. The mineral chemistry of chromian spinel is used to establish the geotectonic setting of ultramafic rocks (e.g. Bonatti and Michael, 1989). Thus, chromian spinels provide a way to distinguish supra-subduction zone (SSZ) from mid-oceanic ridge (MOR) ultramafic–mafic complexes (e.g. Arai et al., 2006; Dare et al., 2009).

The composition of chromian spinels depends on the physicochemical conditions of fractional crystallization and is particularly sensitive to the differences in oxidation state of the mantle (variations in oxygen fugacity) and degree of partial melting in SSZ and MOR environments (e.g. Caran et al., 2010; Dare et al., 2009; Grammatikopoulos et al., 2011; Kapsiotis et al., 2009; Kapsiotis et al., 2011).

Thirty-one ultramafic complexes are known in an E–W trending belt of 60 km length and 5–10 km width in the Haji Abad-Esfandagheh district of the Kerman province in south-east Iran, constituting Iran's

* Corresponding author at: Department of Geology, Payame Noor University, Pajoohesh Square, Kerman, Iran.
E-mail addresses: najafar@yahoo.com, a_najafzadeh@pnu.ac.ir (A.R. Najafzadeh).

http://dx.doi.org/10.1016/j.oregeorev.2015.12.018
0169-1368/

second largest chromite producer after the Faryab (or Asminon) ore deposits (Fig. 1a). These include the Abdasht, Sikhuran, Soghan and Colkahan complexes (Jannessary et al., 2012).

The Abdasht ultramafic complex (McCall, 1985; Jannessary et al., 2012; Najafzadeh and Ahmadipour, 2014b) is exposed in southeastern Iran and hosts podiform chromitite orebodies (collectively known as the Abdasht Mine), which have been mined discontinuously since the 1960s and represent one of the principal Cr sources in Iran. Previous workers (Ahmadipour, 2000; Ahmadipour et al., 2003; Sabzehei, 1974) suggested that the Abdasht chromitites and associated rocks are likely part of mantle diapir (similar to Soghan mafic–ultramafic complex), but they provided no discussion about the petrogenetic significance of the distribution of PGE.

In this study, the Abdasht peridotites and chromitites were investigated through field investigations of geological relationships, petrographic studies, mineral chemistry, and whole-rock geochemistry (platinum-group elements). The paper has two main goals. The first is to determine the origin and tectonic setting of the Abdasht ultramafic complex, and the second is to elucidate the nature of the lithospheric mantle section in the Esfandagheh area. This study provides the first comprehensive description of PGE and their distribution in podiform chromitites and associated rocks from the Abdasht ultramafic complex.

2. Regional geology

The Iran plate was a part of Gondwanaland during the Permian, probably until the Triassic (Wensink, 1981) and subsequently drifted from the Gondwana to join Eurasia. The northern part of the plate was at about its present location relative to Eurasia during the Cretaceous (Lemaire et al., 1997).

Tethyan ophiolites (i.e. Semail-Oman, Kizildag-Turkey, Troodos-Cyprus, etc.) are remnants of oceanic crust and/or supra-subduction zone assemblages that were formed during the closure of the Tethyan Ocean as a result of collision of the Gondwana and Eurasia continents. This closure produced an arcuate ophiolite belt extending from the Balkan Peninsula through Anatolian Taurus Mountains to the Iranian Main Zagros fold-thrust belt (or Main Zagros Thrust Fault) (Dilek et al., 2007). As part of this system, the ~2000 km-long Main Zagros fold-thrust belt, extending from southeastern Turkey through northern Syria and north- northeastern Iraq to western and southern Iran and into northern Oman, is interpreted to have formed during the closure of the Neo-Tethyan Ocean and subsequent oblique collision of the Afro-Arabian plate (Gondwanaland) with the Iranian micro-continent in the Late Cretaceous–Early Tertiary (Alavi, 2004).

The Abdasht ultramafic complex has a north–south trending shape, and is over 8 km long and 5 km wide. It is situated in south-east of

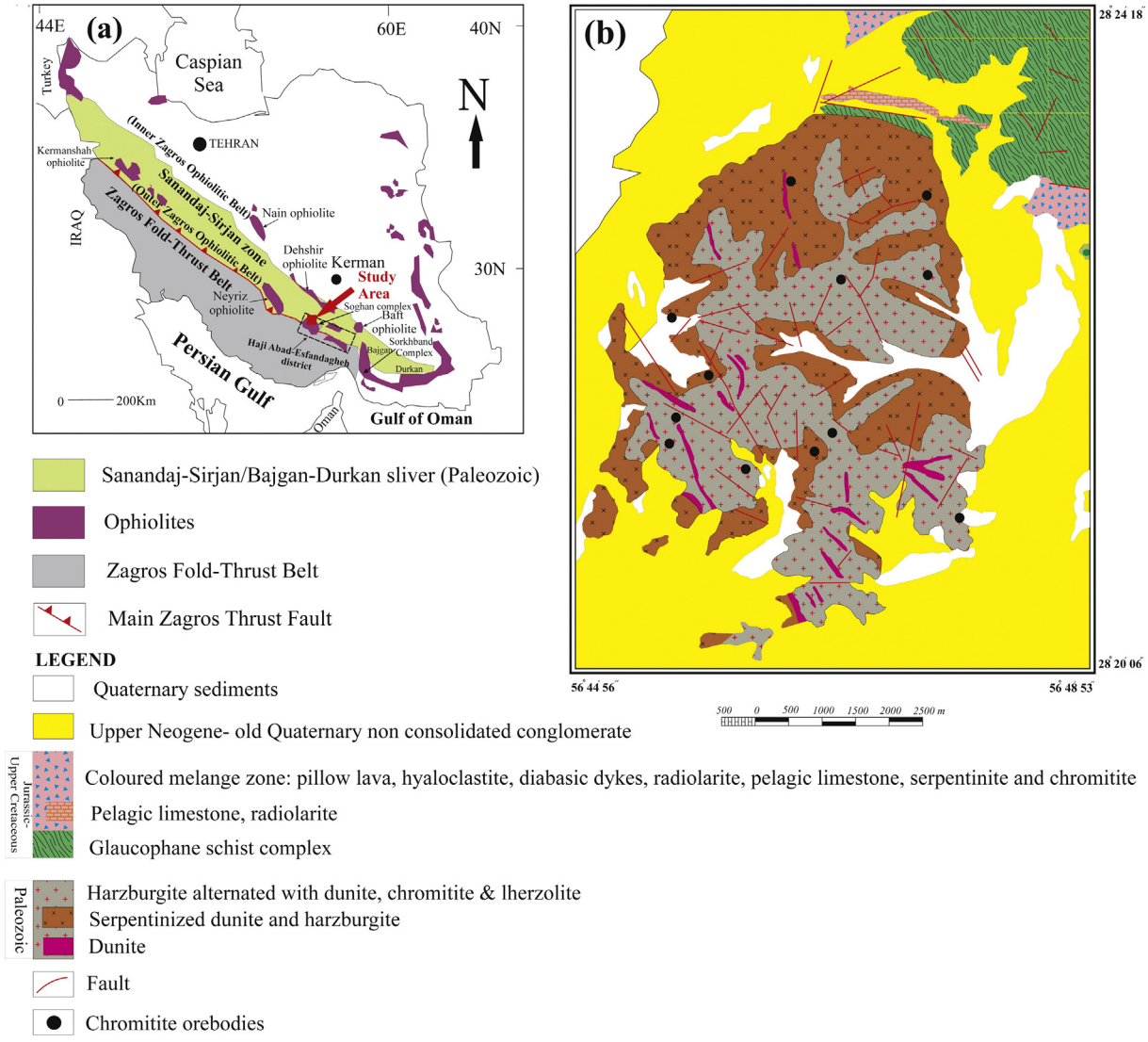

Fig. 1. a) Location of the study area within the Iranian ophiolitic belts and Sanandaj–Sirjan/Bajgan–Durkan (SS/BD) zone. Note the position of the inner (Nain–Dehshir–Baft) and outer (Kermanshah–Neyriz–Haji Abad-Esfandagheh) Zagros ophiolitic belts. b) Simplified geological map of the Abdasht ultramafic complex (modified after Ahmadipour, 2000).

Iran southern Kerman province (Fig. 1a) in the Sanandaj–Sirjan/Bajgan–Durkan (SS/BD) metamorphic zone in the ophiolitic mélange belt of the Haji Abad-Esfandagheh district. The SS/BD block consists of metamorphic rocks (garnetiferous schists, quartzite and marbles) that are Early Paleozoic or older (McCall, 1985). The Bajgan–Durkan complex is believed to be the continuation of the Sanandaj–Sirjan metamorphic zone of Iran and the Bittlis massif of Turkey (McCall, 1985). In this context the Sanandaj–Sirjan microcontinental fragment extends eastwards, and is referred as the Sanandaj–Sirjan/Bajgan–Durkan block (McCall, 1997).

The study area is located in the Haji Abad-Esfandagheh district at the SE edge of the Main Zagros fold-thrust belt (Fig. 1a). This belt resulted from the shortening and accretion of thick sediments from the northern margin of the Arabian platform, essentially behaving as an accretionary prism at the Iranian convergent margin (Shafaii Moghadam and Stern, 2011). The distribution of Upper Cretaceous ophiolites in the Zagros orogenic belt defines the northern limit of the evolving suture between Eurasia and Arabia and marks a Late Cretaceous episode of subduction initiation on the northern side of the Neo-Tethys (Moghadam et al., 2010) and comprises two parallel belts: (1) Outer Zagros Ophiolitic Belt (OB) and (2) Inner Zagros Ophiolitic Belt (IB) (Shafaii Moghadam and Stern, 2011). The OB, crops out along the Zagros fold-thrust belt from the NW to SE (Fig. 1a); it provides a record of the geodynamic evolution of a Neo-Tethys oceanic branch (southern Neo-Tethys Ocean) between the Arabian shield (Gondwana) and the Sanandaj–Sirjan continental block of Iran (e.g. Allahyari et al., 2014; Berberian and King, 1981). The OB contains the Kermanshah, Neyriz and Haji Abad-Esfandagheh ophiolites. The latter have been considered as slices of Tethyan oceanic lithosphere accreted during NE-directed subduction beneath Iran (e.g. Babaie et al., 2001). The IB is located along the SW periphery of the Central Iranian block and contains the Nain–Dehshir–Baft ophiolites (Fig. 1a).

The Haji Abad-Esfandagheh district is located in a very tectonically active zone, composed of highly deformed metamorphic rocks (SS/BD), colored mélange and several mafic–ultramafic complexes (e.g. Soghan (Najafzadeh and Ahmadipour, 2014a); Sikhuran (Ghasemi

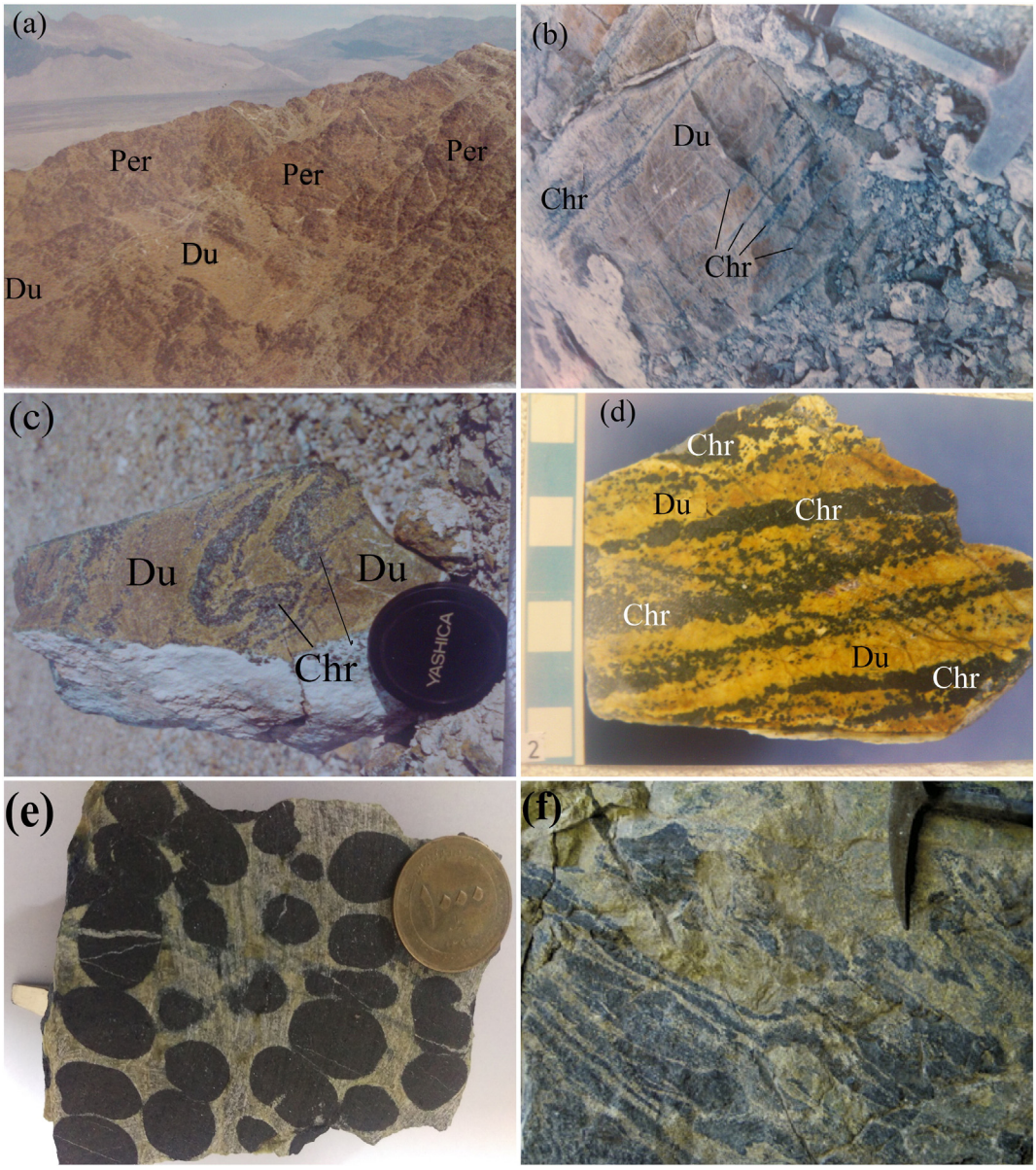

Fig. 2. Field photographs of the chromitites and associated ultramafic rocks from Abdasht ultramafic complex. a) Sharp contact between an envelope of light colored dunite (Du) (hosting the chromitite) and dark massive harzburgitic peridotite (Per). b) Several thin banded units of chromitite (Chr) occur in dunite (Du). c,d) Intrafolial banding of chromitite (Chr) in dunite (Du) due to high P–T deformations. e) Nodular chromitite from the Abdasht mining area; f) Folded schlieren-type chromitite, level 2, Abdasht mining area, (after Jannessary et al., 2012).

et al., 2002); Dehsheikh (Peighambari et al., 2011) and Abdasht (Jannessary et al., 2012; Najafzadeh and Ahmadipour, 2014b)) with total probable reserves of 8 million t of chromite ores grading 41% Cr_2O_3. The Abdasht complex is one of the ultramafic massifs in Haji Abad-Esfandagheh district within the Outer Zagros Ophiolitic Belt (Fig. 1a, b).

3. Field observations

The Abdasht complex is one of the major ultramafic complexes in south-east Iran (located in Esfandagheh area from the Haji Abad-Esfandagheh district) and is composed mainly of serpentinized harzburgite, dunite, chromitite, and subordinate lherzolite and wehrlite. The peridotites are exposed as discontinuous layers, pods and elongated lenses. The layers are up to 25 m in thickness and exhibit fold and thrust structures. The degree of serpentinization is up to 50 vol.%.

Harzburgites are the most abundant rock type exposed within the complex (more than 70%). They are observed as dark brown-colored outcrops that contain deformed and elongated cm-sized orthopyroxenes and sparse mm-sized chromian spinels (Fig. 2a).

The dunites are surrounded by harzburgites and occur as small pods to elongated lenses and relatively extended deformational layers and range in extension from a few m to a few km (e.g. in Abdasht Mine). The contacts between harzburgites and dunites are sharp, but the original structural geometry of the harzburgites and dunites has been obliterated by extensive faulting and deformation.

The Abdasht ultramafic complex contains several chromitite ore bodies. In all of the types of chromitite ore bodies (massive, banded or nodular) the contacts between the ores and the host dunites are sharp. In rare instances, such as in Kamal-Abad banded ores, the contact is gradational. Occasionally, the chromitite bands display folding. The chromitite ore bodies follow three distinct pseudo-stratigraphic levels that occur in 16 mineralized outcrops up to 3 km long. Some of these locations are actively mined and all of them belong to the concordant, deformed podiform type. In 1969, reserves of 0.5–1 million t of ore were indicated (Schmidt, 1974). At that time, about 130 t per day of ore (grading 52% Cr_2O_3) was mined at three levels connected by a shaft inclined at 48°. According to Hillebrand (1983), the main ore body extends for 1000 m along strike and dips 40 to 60° north. Some of the massive chromitite lenses are 10 to 25 m long and 0.5–3 m thick. In 2005, production took place in ore body 1 on level 8 at 220 m depth. This level 1 ore body at Abdasht Mine consists of strongly deformed ore with ore boudins reaching 3 m in thickness (Jannessary et al., 2012). The mineral bands occur as lenses and tabular (layered) shapes of variable sizes (Fig. 2b). Chromitite layers occasionally show intrafolial folding due to high P–T deformation (Fig. 2c-d). The level 1 chromitite illustrates abundant undeformed nodular that extends along the south-western border of the complex. Nodular chromitite ores contain rounded matrix-supported chromite nodules in a moderately serpentinized dunite host. The sizes of nodules vary from 0.5 to 2.5 cm in diameter (Fig. 2e). The nodules are internally massive and contain interlocking anhedral chromian spinel grains.

A small active mine in the centre of the Abdasht complex exploits a steeply inclined folded schlieren-type chromitite attributed to the stratigraphic position of the level 2 chromitite (Fig. 2f). The level 3 chromitite exposes the stratigraphic footwall in the area along the eastern border of the complex, with boudin-shaped lenses of 0.5 to 3 m thickness that can be traced for 3 km along strike (Jannessary et al., 2012).

The boundaries between chromitite and dunites are commonly well defined. The tabular or layer shapes are developed parallel to the peridotite banding and their lateral extent reaches up to 600 m (e.g. in Abdasht Mine, Shabahang and Kamal Abad). In these ore bodies, chromitites exhibit fine-grained disseminations of chromian spinel through to coarse-grained nodular to massive coarse-grained nodular chromitite ores. Chromitite varies from disseminated into massive and the thickness of chromitite layers increases to reach 4 m in the deepest part of the mineral zone. In some of the mines (e.g. the Six Mine) there are high-grade massive chromitite lenses that are located in the serpentinized marginal parts of the complex.

4. Petrography of peridotites and chromitite orebodies

The harzburgites contain olivine (74–88 vol.%) ($Fo_{90.7-91.1}$), orthopyroxene (11–25 vol.%) ($En_{90-93}Fs_{6-9}Wo_1$), rare (up to 3 vol.%) clinopyroxene and chromian spinel (up to 1 vol.%) (Fig. 3). They have a protogranular texture and the grain size of olivine and orthopyroxene is up to 1 cm (Fig. 4a). Olivine sometimes shows a resorbed texture when it is enclosed by large orthopyroxene grains (Fig. 4b). In other samples, porphyroclastic textures are defined by orthopyroxene grains. Orthopyroxene can host clinopyroxene lamellae and shows deformational features such as elongation and the development of kink bands. Chromian spinel (0.1–1 mm in diameter) is brown to reddish brown-colored and euhedral to subhedral and in some cases, a Cr-rich chlorite (kaemmererite) rim is developed around chromian spinel crystal (Fig. 4c). High P–T textures such as elongation of orthopyroxenes and spinels, mechanical twining in olivines, exsolution lamellae in

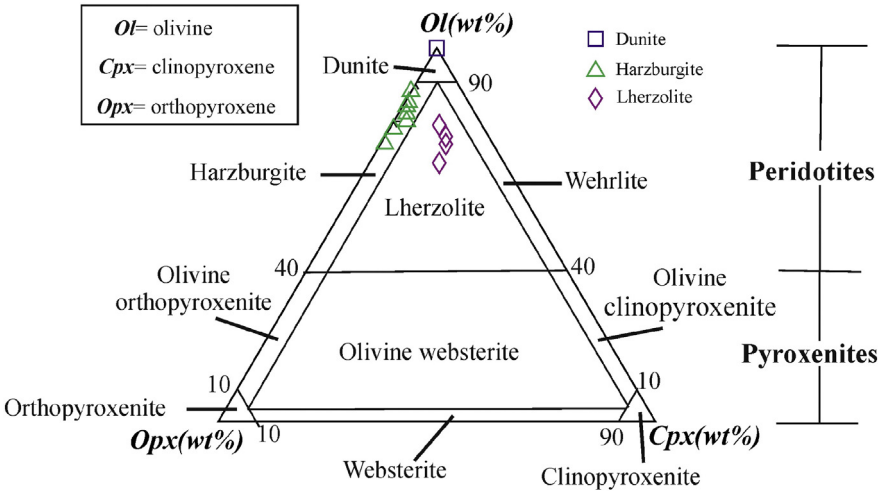

Fig. 3. Modal mineralogy based on petrographic investigation of the peridotites from the Abdasht Ultramafic Complex. Classification diagram of ultramafic rocks is after Le Maitre (2002).

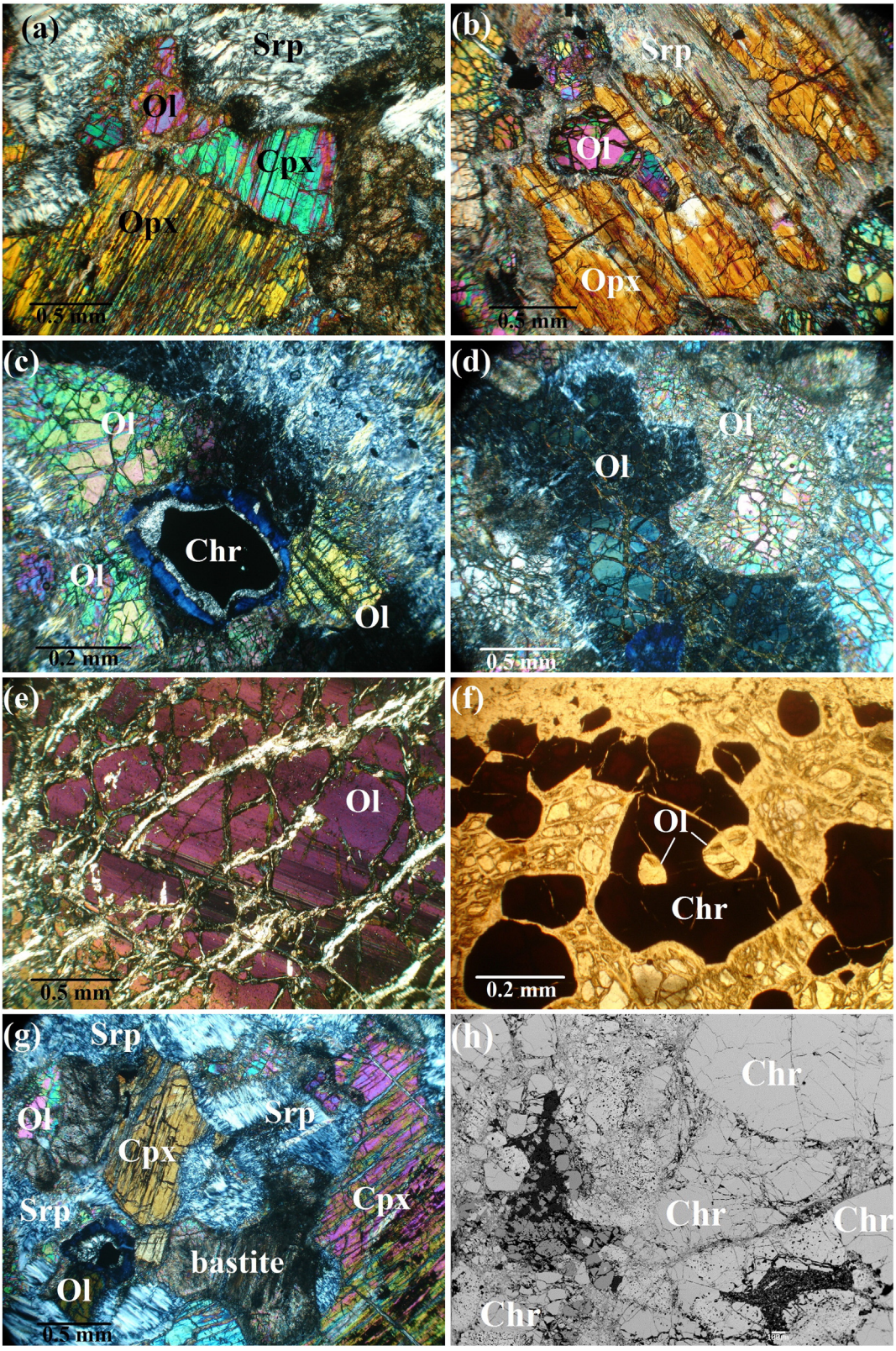

Fig. 4. Photomicrographs of harzburgites, dunites and lherzolites from the Abdasht ultramafic complex. TPL = transmitted polarized light; TCN = transmitted crossed nicols. a) Clinopyroxene (Cpx) grains in a serpentinized (Srp) matrix in harzburgite with protogranular texture (TCN). b) Resorbed olivine (Ol) in a large orthopyroxene (Opx) grain partly altered to serpentine (Srp) in harzburgite (TCN). c) Chromian spinel (Chr) grain show rims of Cr-rich chlorite (kaemmererite) in a partly serpentinized olivine (Ol) matrix in harzburgite (TCN). d) Grain boundary migration in partly serpentinized olivines (Ol) of dunite (TCN). e) Internal deformation and kink band in partly serpentinized olivines of dunite (TCN). f) Subhedral chromian spinel grain (Sp) hosting two olivine inclusions (Ol) in dunite (TPL). g) Protogranular serpentine bastite after orthopyroxene showing the ragged, embayed appearance of orthopyroxene in lherzolite (TCN). h) Back-scattered electron (BSE) images of unaltered chromian spinel grains with the matrix filled by serpentine from massive chromitites.

Table 1
Representative electron-microprobe analyses of chromian spinel in different chromitite pods of the Abdasht ultramafic complex, Iran.

Sample no.	Ab3	Ab3	Ab4	Ab4	Ab4	Ab7	Ab7	Ab7
Oxides (wt.%)								
SiO_2	bdl	0.01	bdl	bdl	bdl	0.01	bdl	bdl
TiO_2	0.16	0.14	0.18	0.15	0.17	0.16	0.18	0.20
Al_2O_3	12.20	12.40	12.00	12.80	12.10	12.50	12.60	12.07
Cr_2O_3	59.20	59.10	59.00	58.97	60.10	59.20	59.80	59.20
Fe_2O_3	0.56	0.70	0.80	1.10	1.00	0.60	1.20	0.90
FeO	13.70	13.20	13.50	13.20	13.10	13.20	13.50	13.20
MnO	bdl	bdl	bdl	bdl	bdl	bdl	bdl	bdl
MgO	13.20	13.80	13.40	13.50	13.10	13.40	13.50	13.00
CaO	0.00	0.00	0.00	0.00	0.00	0.00	0.00	0.00
NiO	0.06	0.09	0.07	0.07	0.05	0.01	0.08	0.08
Total	99.08	99.44	98.95	99.79	99.62	99.08	100.86	98.65
Cations (structural formula on the basis of 4 oxygen)								
Si	bdl	0.000	bdl	bdl	bdl	0.000	bdl	bdl
Ti	0.004	0.003	0.004	0.004	0.004	0.004	0.004	0.005
Al	0.465	0.469	0.458	0.482	0.458	0.474	0.471	0.462
Cr	1.512	1.500	1.509	1.490	1.526	1.507	1.498	1.519
Fe^{3+}	0.014	0.017	0.019	0.026	0.024	0.015	0.029	0.022
Fe^{2+}	0.370	0.354	0.365	0.353	0.352	0.355	0.358	0.358
Mn	bdl	bdl	bdl	bdl	bdl	bdl	bdl	bdl
Mg	0.636	0.660	0.646	0.643	0.627	0.643	0.638	0.629
Ca	bdl	bdl	bdl	bdl	bdl	bdl	bdl	bdl
Ni	0.002	0.002	0.002	0.002	0.001	0.000	0.002	0.002
Total	3.001	3.004	3.002	2.997	2.992	2.998	2.997	2.994
Cr/Al	3.26	3.20	3.30	3.09	3.33	3.18	3.18	3.29
[a]Cr#	0.77	0.76	0.77	0.76	0.77	0.76	0.76	0.77
[b]Fe#	0.37	0.35	0.36	0.35	0.36	0.36	0.36	0.36
[c]Mg#	0.63	0.65	0.64	0.65	0.64	0.64	0.64	0.64
[d]Fe^{3+}#	0.01	0.01	0.01	0.01	0.01	0.01	0.01	0.01
[e]$(FeO/MgO)_{melt}$	0.65	0.60	0.63	0.61	0.63	0.62	0.63	0.64
[f]$Al_2O_{3\ melt}$	12.00	12.09	11.92	12.25	11.96	12.13	12.17	11.95
[f]$TiO_{2\ melt}$	0.26	0.23	0.28	0.25	0.27	0.26	0.28	0.31

bdl: below detection limit.
[a] Cr#:Cr/(Cr + Al) atomic ratio.
[b] Mg#: Mg/(Mg + Fe^{2+}) atomic ratio.
[c] Fe#:Fe^{2+}/(Fe^{2+} + Mg) atomic ratio.
[d] Fe^{3+}#: Fe^{3+}/(Fe^{3+} + Al + Cr) atomic ratio.
[e] Maurel (1984, cited in Augé, 1987).
[f] Rollinson (2008) for arc settings.

the orthopyroxenes and other plastic deformational features in harzburgites indicate that these rocks were originally formed at mantle pressures and temperatures.

Dunites consist of olivine (95–99 vol.%) ($Fo_{91.3–91.9}$), and chromian spinel (1–5 vol.%) (Fig.3). These minerals have a granoblastic texture. Olivine has a curved grain boundary and there is evidence for grain boundary migration (GBM) recrystallisation (Fig. 4d). Olivine displays deformation lamellae along its slip planes, mini kinking as mechanical twinnings and irregular extinction band configurations (Fig. 4e). Finer-grained strain-free polygonized olivine crystals probably indicate static recrystallisation processes in dunites. Olivine grains range from 0.5 to a few millimiters in diameter. Chromian spinels are finer-grained at 0.1–0.3 mm in diameter and occur as subhedral to euhedral dark brown grains and locally host olivine inclusions (Fig. 4f).

Lherzolites contain 66–79 vol.% olivine ($Fo_{90.7–91.1}$), up to 11–18 vol.% clinopyroxene ($En_{48–50}Fs_{1-3}Wo_{49–50}$), 10–15 vol.% orthopyroxene ($En_{91–92}Fs_{7–8}Wo_1$) and about 1 vol.% chromian spinel (Fig. 3). Protogranular texture is prevalent in lherzolites and deformational features such as kink band and undulatory extinction are frequent in olivine grains. Clinopyroxene shows a range in grain size from 0.5–1 mm. The coarse crystals sometimes contain exsolution lamellae of orthopyroxene. The lherzolites are highly serpentinized and orthopyroxene bastites are commonly developed (Fig. 4g). In some cases the lherzolites containchromian spinel grains that are partially or completely surrounded by Cr-rich chlorite (kaemmererite) (Fig. 4g); this texture is also developed in the harzburgites.

Massive chromitite ores composed of 80–90 vol.% chromian spinel and minor serpentinized olivine is found between the spinel grains. The grain sizes of chromian spinels ranges from 5 to 15 mm in these ore bodies. The massive chromitite is enclosed in dunite, but their boundaries and shapes are commonly interrupted by numerous faults. They consist of euhedral to subhedral chromian spinel and interstitial serpentinized olivines. Chromian spinel crystals have fractures with no alteration (Fig. 4h).

In disseminated chromitites, chromian spinels are small euhedral grains (with 2–3 mm in diameter) set in olivine matrix. Sometimes chromian spinels have small rounded olivine inclusions. In the Kamal Abad Mine, chromitites show a banded texture defined by fine-grained chromitite intercalated with serpentinized dunite (Fig. 2d). In the Momtaz Mine, nodular chromitites are rounded and flattened and chromite nodules hosted by a dunite matrix (Fig. 2e).

5. Methods and analytical procedures

The analysis of chromian spinel and associated silicate minerals was carried out with a JEOL electron-probe micro analyzer CAMEBAX SX50 at the Jusieu and Bertagne Occidentale University, France. Analytical conditions were 15 kV accelerating voltage, 12 nA probe current with the counting time varying from 10 to 20 s., and the raw data were corrected with an on-line ZAF program. The amounts of Fe^{3+} and Fe^{2+} in chromian spinel were calculated assuming spinel (AB_2O_4) stoichiometry, based on the general equation of Droop (1987) for calculating ferric iron. The analytical results are presented in Tables 1, 2, 3 and 4.

A total of 15 representative samples of chromitites and associated dunites, harzburgites, and lherzolites of the ultramafic complex of Abdasht were selected and analyzed for all PGE (Os, Ir, Ru, Rh, Pt, and Pd), Au, Ni and Cu. The very low PGE and Au contents impose the use of a combined procedure of pre-concentration and matrix elimination prior to the detection with ICP-MS. This was achieved by fire assay with nickel sulfide collection (mixing the sample with mixture of soda ash, borax, silica sulfur and nickel carbonate or nickel oxide). After pre concentration the sample solution were analyzed using Perkin-Elmer Sciex ELAN 9000 ICPMS at the Genalysis Laboratory Services Pty. Ltd. at Maddington, Western Australia. Analytical accuracy and precision were routinely checked using international standards, including AMIS0076, AMIS0124, HGMN.1, and by analyzing blanks and duplicates. Based on reference samples analyzed during several years in the lab recovery was estimated to be better than 85%, which is in the range of the efficiency usually obtained by NiS fire assay. Detection limits are 2 ppb for Os, Ir, Ru, Pt, Pd and Ni, 1 ppb for Rh and Cu and 5 ppb for Au.

6. Mineral and whole rock compositional variations of the chromitites and associated rocks

Ahmadipour et al. (2003) studied the geochemistry, petrology and mineralogy of the chromitites and associated peridotites from the Abdasht ultramafic complex. Here we emphasize some features (such as mineral chemistry and bulk-rock PGE geochemistry) that are important to the interpretation of the distribution of PGE. Sixty one (61) electron microprobe analyses were carried out on chromian spinel and silicates from polished sections from chromitite, and the host dunite, harzburgite and lherzolite. Electron probe micro analyses of chromian spinel, olivine, orthopyroxene and clinopyroxene are given in Tables 1-4. The whole rock PGE contents of chromitites and peridotites together with Pd/Ir values and Pt anomaly ($Pt/Pt^* = Pt_n/\sqrt{Rh_n \cdot Pd_n}$) are listed in Table 5.

6.1. Mineral chemistry

6.1.1. Chromian spinel (Cr-spinel) composition

There is a distinct compositional difference in chromian spinel chemistry from the different rock types of the Abdasht complex. The chromian spinels are usually fresh, well-preserved and retained their

Table 2
Representative electron-microprobe analyses of accessory chromian spinel from the Abdasht peridotites. Du: accessory chromian spinel in dunite, Hz: accessory chromian spinel in harzburgite, Lz: accessory chromian spinel in lherzolite.

Lithology	Du	Du	Du	Du	Du	Du	Du	Du	Du	Du	Hz
Sample no.	Ab2	Ab2	Ab5	Ab5	Ab5	Ab2	Ab2	Ab2	Ab5	Ab5	Ab1
Oxides (wt.%)											
SiO_2	bdl	bdl	0.01	bdl	bdl	0.01	0.02	0.02	0.01	0.01	bdl
TiO_2	0.10	0.11	0.09	0.08	0.12	0.08	0.11	0.14	0.10	0.12	0.06
Al_2O_3	7.10	6.50	6.70	6.30	6.20	6.87	6.50	6.76	6.21	6.35	27.40
Cr_2O_3	52.10	52.30	52.00	52.60	52.40	55.21	57.41	58.12	59.31	58.37	39.40
Fe_2O_3	5.60	5.10	5.30	5.40	5.00	2.54	1.54	1.63	2.05	2.72	1.70
FeO	25.10	25.20	24.80	26.10	25.40	23.96	22.98	23.25	22.50	22.20	17.00
MnO	0.21	0.22	0.23	0.22	0.21	0.10	0.00	0.10	0.10	0.10	0.22
MgO	5.40	5.60	5.50	5.20	5.80	6.28	7.34	7.81	8.10	7.86	12.00
CaO	bdl	bdl	bdl	bdl	0.01	0.03	0.02	0.03	bdl	bdl	bdl
NiO	0.04	0.05	0.01	0.05	0.02	0.01	0.05	0.05	0.04	0.02	0.10
Total	95.65	95.08	94.64	95.95	95.16	95.09	95.97	97.91	98.42	97.75	97.88
Cations (structural formula on the basis of 4 oxygen)											
Si	bdl	bdl	bdl	bdl	bdl	bdl	0.001	0.001	bdl	bdl	bdl
Ti	0.003	0.003	0.002	0.002	0.003	0.002	0.003	0.004	0.003	0.003	0.001
Al	0.304	0.281	0.290	0.271	0.268	0.294	0.274	0.279	0.255	0.262	0.998
Cr	1.497	1.517	1.512	1.519	1.520	1.586	1.626	1.610	1.634	1.618	0.962
Fe^{3+}	0.153	0.141	0.147	0.148	0.138	0.069	0.042	0.043	0.054	0.072	0.040
Fe^{2+}	0.763	0.773	0.763	0.797	0.780	0.728	0.688	0.681	0.656	0.651	0.439
Mn	0.006	0.007	0.007	0.007	0.007	0.003	0.000	0.003	0.003	0.003	0.006
Mg	0.293	0.306	0.301	0.283	0.317	0.340	0.392	0.408	0.421	0.411	0.553
Ca	bdl	bdl	bdl	bdl	0.000	0.001	0.001	0.001	bdl	bdl	bdl
Ni	0.001	0.001	0.000	0.001	0.001	0.000	0.001	0.001	0.001	0.001	0.002
Total cations	3.020	3.028	3.023	3.028	3.033	3.023	3.026	3.029	3.026	3.020	2.999
Cr/Al	4.92	5.40	5.21	5.60	5.67	5.39	5.93	5.77	6.41	6.17	0.96
[a]Cr#	0.83	0.84	0.84	0.85	0.85	0.84	0.86	0.85	0.87	0.85	0.49
[b]Mg#	0.28	0.28	0.28	0.26	0.29	0.32	0.36	0.37	0.39	0.39	0.56
[c]Fe#	0.72	0.72	0.72	0.74	0.71	0.68	0.68	0.63	0.61	0.61	0.44
[d]Fe^{3+}#	0.08	0.07	0.08	0.08	0.07	0.04	0.02	0.02	0.03	0.04	0.02

Lithology	Hz	Hz	Hz	Hz	Hz	Hz	Hz	Hz	Lz	Lz	Lz	Lz
Sample no.	Ab1	Ab1	Ab6	Ab6	Ab1	Ab1	Ab6	Ab6	Ab9	Ab9	Ab9	Ab9
Oxides (wt.%)												
SiO_2	0.01	0.02	bdl	bdl	bdl	0.03	0.01	0.03	bdl	bdl	0.01	bdl
TiO_2	0.04	0.09	0.03	0.06	0.03	0.04	0.02	0.08	0.06	0.07	0.04	0.05
Al_2O_3	27.30	27.50	27.10	27.80	21.57	19.81	20.45	27.50	26.80	27.50	27.10	26.50
Cr_2O_3	39.20	38.40	39.10	39.00	46.62	44.20	43.25	39.10	38.50	39.20	38.60	39.00
Fe_2O_3	1.50	1.01	0.70	1.74	2.67	3.84	2.96	2.10	1.22	1.54	1.22	2.31
FeO	17.20	17.90	17.40	17.11	16.28	16.43	16.83	16.90	17.10	17.50	17.10	16.90
MnO	0.26	0.22	0.20	0.19	0.10	0.16	0.18	0.21	0.22	0.23	0.21	0.20
MgO	12.20	12.10	12.30	12.20	11.84	11.52	11.35	12.00	12.30	12.40	12.30	12.04
CaO	bdl	bdl	bdl	0.02	0.01	0.02	bdl	bdl	bdl	bdl	0.02	bdl
NiO	0.05	0.07	0.06	0.04	0.04	0.06	0.05	0.04	0.04	0.02	0.03	0.07
Total	97.76	97.31	96.89	98.16	99.16	96.11	95.10	97.96	96.24	98.46	96.63	97.07
Si	0.000	0.001	bdl	bdl	bdl	0.001	0.000	0.001	bdl	bdl	0.000	bdl
Ti	0.001	0.002	0.001	0.001	0.001	0.001	0.000	0.002	0.001	0.002	0.001	0.001
Al	0.995	1.008	0.997	1.007	0.795	0.760	0.790	0.999	0.992	0.995	0.998	0.976
Cr	0.959	0.944	0.965	0.948	1.153	1.137	1.121	0.953	0.956	0.952	0.954	0.963
Fe^{3+}	0.035	0.024	0.016	0.040	0.063	0.094	0.073	0.049	0.029	0.036	0.029	0.054
Fe^{2+}	0.445	0.465	0.454	0.440	0.426	0.447	0.462	0.436	0.449	0.449	0.447	0.442
Mn	0.007	0.006	0.005	0.005	0.003	0.004	0.005	0.005	0.006	0.006	0.006	0.005
Mg	0.563	0.561	0.572	0.559	0.552	0.559	0.555	0.552	0.576	0.568	0.573	0.561
Ca	bdl	bdl	bdl	0.001	0.000	0.001	bdl	bdl	bdl	bdl	0.001	bdl
Ni	0.001	0.002	0.002	0.001	0.001	0.002	0.001	0.001	0.001	0.000	0.001	0.002
Total	3.004	3.010	3.010	3.001	2.993	3.003	3.007	2.997	3.010	3.007	3.008	3.002
Cr/Al	0.96	0.94	0.97	0.94	1.45	1.50	1.42	0.95	0.96	0.96	0.96	0.99
Cr#	0.49	0.48	0.49	0.49	0.59	0.60	0.59	0.49	0.49	0.49	0.49	0.50
Mg#	0.56	0.55	0.56	0.56	0.57	0.56	0.55	0.56	0.56	0.56	0.56	0.56
Fe#	0.44	0.45	0.44	0.44	0.44	0.45	0.45	0.44	0.44	0.44	0.44	0.44
Fe^{3+}#	0.02	0.01	0.01	0.02	0.03	0.05	0.04	0.02	0.01	0.02	0.01	0.03

bdl: below detection limit.
[a] Cr#:Cr/(Cr + Al) atomic ratio.
[b] Mg#: Mg/(Mg + Fe^{2+}) atomic ratio.
[c] Fe#:Fe^{2+}/(Fe^{2+} + Mg) atomic ratio.
[d] Fe^{3+}#: Fe^{3+}/(Fe^{3+} + Al + Cr) atomic ratio.

primary compositions. Microprobe analyses of chromian spinels in chromitites and peridotites are presented in Tables 1 and 2, respectively. There is no evidence of compositional variation or zoning in chromian spinels of chromitites (Fig. 4h). The composition of chromian spinels in massive chromitites yields Cr_2O_3 from 59 to 60.1 wt.% (average 59.3 wt.%), Al_2O_3 from 12.0 to 12.8 wt.% (average 12.3 wt.%) and MgO

Table 3
Representative analyses of olivine from the pridotites in the Abdasht ultramafic complex. Du: Dunite, Hz: Harzburgite, Lz: Lherzolite.

Lithology	Du	Du	Du	Du	Du	Du	Hz	Hz	Hz	Hz	Hz	Hz	Hz	Lz	Lz	Lz
Sample no.	Ab2	Ab2	Ab5	Ab5	Ab5	Ab5	Ab1	Ab1	Ab1	Ab6	Ab6	Ab6	Ab6	Ab9	Ab9	Ab9
SiO_2	41.40	40.90	41.10	41.00	41.03	41.00	41.08	40.50	41.50	40.80	41.80	42.00	41.70	40.80	41.09	41.10
TiO_2	0.02	0.01	0.03	0.05	0.01	0.02	bdl	0.01	bdl	0.04	0.01	bdl	0.01	0.02	bdl	bdl
Al_2O_3	bdl	bdl	0.01	0.01	bdl	0.01	0.01	0.02	bdl	0.03	0.01	0.01	0.02	bdl	bdl	0.01
Cr_2O_3	0.02	bdl	bdl	bdl	bdl	0.03	0.02	0.05	0.01	bdl	bdl	0.01	0.02	bdl	bdl	0.02
Fe_2O_3	1.03	1.68	1.77	2.09	1.51	2.23	1.40	2.08	0.89	2.00	bdl	bdl	0.12	0.68	bdl	1.01
FeO	7.08	6.59	6.40	6.52	6.84	6.50	7.24	7.23	8.20	6.70	7.80	8.50	8.79	8.29	8.50	8.19
MnO	0.15	0.12	0.08	0.12	0.13	0.14	0.10	0.16	0.08	0.10	0.16	0.11	0.12	0.12	0.15	0.10
MgO	51.01	50.80	51.20	51.02	50.80	51.20	50.60	49.90	50.40	50.60	50.40	49.60	50.20	49.60	49.50	50.10
CaO	0.01	0.04	0.01	bdl	bdl	0.01	bdl	bdl	0.01	0.02	0.03	bdl	bdl	0.01	bdl	0.01
NiO	0.34	0.33	0.36	0.39	0.32	0.31	0.35	0.39	0.38	0.40	0.35	0.39	0.37	0.28	0.23	0.30
Na_2O	bdl	bdl	bdl	bdl	0.01	bdl	bdl	bdl	0.01	bdl	bdl	bdl	bdl	bdl	bdl	bdl
K_2O	0.01	bdl	bdl	bdl	bdl	bdl	bdl	bdl	bdl	bdl	bdl	0.01	bdl	bdl	bdl	bdl
Total	101.06	100.47	100.97	101.20	100.65	101.44	100.80	100.34	101.48	100.69	100.56	100.63	101.35	99.80	99.47	100.84
Si	0.997	0.991	0.990	0.988	0.993	0.985	0.994	0.988	0.999	0.988	1.012	1.020	1.005	0.999	1.008	0.996
Ti	0.000	0.000	0.001	0.001	0.000	0.000	bdl	0.000	bdl	0.001	0.000	bdl	0.000	0.000	bdl	bdl
Al	bdl	bdl	0.000	0.000	bdl	0.000	0.000	0.001	0.000	0.001	0.000	0.000	0.001	bdl	bdl	0.000
Cr	0.000	bdl	bdl	bdl	bdl	0.001	0.000	0.001	0.000	bdl	bdl	0.000	0.000	bdl	bdl	0.000
Fe^{2+}	0.160	0.160	0.160	0.170	0.170	0.170	0.180	0.190	0.190	0.180	0.160	0.173	0.177	0.180	0.174	0.190
Mn	0.003	0.002	0.002	0.002	0.003	0.003	0.002	0.003	0.002	0.002	0.003	0.002	0.002	0.002	0.003	0.002
Mg	1.831	1.835	1.839	1.832	1.832	1.834	1.825	1.814	1.809	1.827	1.819	1.796	1.804	1.810	1.810	1.810
Ca	0.000	0.001	0.000	bdl	bdl	0.000	bdl	bdl	0.000	0.001	0.001	bdl	bdl	0.000	bdl	0.000
Ni	0.007	0.006	0.007	0.008	0.006	0.006	0.007	0.008	0.007	0.008	0.007	0.008	0.007	0.006	0.005	0.006
Na	bdl	bdl	bdl	bdl	bdl	bdl	bdl	bdl	bdl	bdl	bdl	bdl	bdl	bdl	bdl	bdl
K	bdl	bdl	bdl	bdl	bdl	bdl	bdl	bdl	bdl	bdl	bdl	bdl	bdl	bdl	bdl	bdl
Total	3.000	3.000	3.000	3.000	3.000	3.000	3.000	3.000	3.000	3.000	3.000	3.000	3.000	3.000	3.000	3.000
Fo	91.76	91.63	91.85	91.43	91.57	91.34	91.29	90.57	90.81	91.27	91.82	91.12	90.84	90.73	91.07	90.65
Fa	8.07	8.20	8.05	8.44	8.29	8.51	8.60	9.27	9.10	8.60	7.97	8.76	9.03	9.13	8.77	9.24

from 13.0 to 13.8 wt.% (average 13.4 wt.%). In the massive chromitites, chromian spinels are Cr-rich and exhibit a uniform composition. They are characterized by Cr# [$=Cr/(Cr + Al)$ atomic ratio] ranging from 0.76 to 0.77, Mg# [$=Mg/(Mg + Fe^{2+})$ atomic ratio] from 0.63 to 0.65, whereas TiO_2 is <0.2 wt.% (average 0.17 wt.%) (Fig. 5a). All spinels exhibit negative correlation between the Al_2O_3 versus Cr_2O_3, and MgO

Table 4
Representative microprobe analyses of orthopyroxene and clinopyroxene from the studied harzburgites and lherzolites. Mg#:$Mg/(Mg + Fe^{2+})$, $En = 100 \times Mg/(Mg + Fe^{2+} + Ca)$, $Fs = 100 \times Fe^{2+}/(Mg + Fe^{2+} + Ca)$, $Wo = 100 \times Ca/(Mg + Fe^{2+} + Ca)$, OPX = Orthopyroxene, CPX = Clinopyroxene, Hz = Harzburgite, Lz = Lherzolite, bdl = below detection limit.

Mineral	OPX	OPX	OPX	OPX	OPX	OPX	OPX	OPX	OPX	CPX	CPX	CPX	CPX
Lithology	Hz	Hz	Hz	Hz	Hz	Hz	Lz	Lz	Lz	Lz	Lz	Lz	Lz
Sample No.	Ab1	Ab1	Ab1	Ab6	Ab6	Ab6	Ab9	Ab9	Ab9	Ab9	Ab9	Ab9	Ab9
SiO_2	56.50	56.70	56.60	56.20	56.80	56.10	56.20	56.40	56.70	51.62	51.30	52.00	52.60
TiO_2	bdl	0.01	0.02	0.03	0.01	0.00	0.04	0.03	0.04	0.25	0.31	0.26	0.32
Al_2O_3	2.10	2.30	1.80	2.00	2.20	1.60	2.60	2.80	2.90	3.50	3.70	3.25	3.20
Cr_2O_3	0.61	0.51	0.54	0.50	0.51	0.49	0.50	0.51	0.50	0.45	0.65	0.52	0.60
FeO_t	5.50	5.60	5.40	5.90	5.70	5.70	5.50	5.40	5.60	3.10	2.95	2.65	2.00
MnO	0.11	0.14	0.07	0.09	0.11	0.12	0.60	0.12	0.10	0.10	0.08	0.10	0.10
MgO	34.80	34.50	34.70	35.10	34.10	34.20	34.00	34.20	33.80	17.00	17.21	17.23	16.64
CaO	0.35	0.39	0.38	0.37	0.38	0.35	0.61	0.60	0.59	23.35	23.10	23.56	23.58
Na_2O	bdl	0.01	0.02	bdl	0.01	0.02	0.05	0.04	0.03	0.11	0.12	0.11	0.13
K_2O	bdl	bdl	bdl	bdl	bdl	0.01	bdl	bdl	bdl	bdl	bdl	bdl	bdl
NiO	0.08	0.05	0.12	0.11	0.14	0.09	0.16	0.18	0.10	0.01	0.00	0.12	0.14
Total	100.05	100.21	99.65	100.30	99.96	98.68	100.26	100.28	100.36	99.49	99.42	99.80	99.31
Si	1.940	1.946	1.952	1.925	1.958	1.956	1.932	1.935	1.947	1.885	1.873	1.891	1.925
Ti	bdl	bdl	0.001	0.001	bdl	bdl	0.001	0.001	0.001	0.007	0.009	0.007	0.009
Al^4	0.060	0.054	0.048	0.075	0.042	0.044	0.067	0.064	0.052	0.108	0.119	0.102	0.066
Al^6	0.025	0.040	0.025	0.006	0.048	0.022	0.038	0.049	0.066	0.042	0.040	0.038	0.072
Fe^{3+}	0.018	0.001	0.009	0.055	0.000	0.011	0.019	0.004	0.000	0.061	0.068	0.057	0.000
Cr	0.017	0.014	0.015	0.014	0.014	0.014	0.014	0.014	0.014	0.013	0.019	0.015	0.017
Fe^{2+}	0.140	0.160	0.146	0.114	0.164	0.156	0.140	0.151	0.161	0.034	0.022	0.024	0.061
Mn	0.003	0.004	0.002	0.003	0.003	0.004	0.017	0.003	0.003	0.003	0.002	0.003	0.003
Mg	1.782	1.765	1.784	1.792	1.752	1.778	1.742	1.749	1.731	0.925	0.937	0.934	0.908
Ca	0.013	0.014	0.014	0.014	0.014	0.013	0.022	0.022	0.022	0.914	0.903	0.918	0.925
Na	bdl	0.001	0.001	bdl	0.001	0.001	0.003	0.003	0.002	0.008	0.008	0.008	0.009
Tot. cat	4.000	4.000	4.000	4.000	4.000	4.000	4.000	4.000	4.000	4.000	4.000	4.000	4.000
Mg#	0.93	0.92	0.92	0.94	0.91	0.92	0.93	0.92	0.91	0.96	0.98	0.98	0.94
Wo	0.67	0.74	0.72	0.71	0.73	0.67	1.18	1.15	1.13	48.78	48.53	48.93	48.83
En	92.08	91.01	91.75	93.34	90.76	91.33	91.49	91.01	90.46	49.41	50.31	49.79	47.94
Fs	7.26	8.25	7.53	5.95	8.51	8.00	7.33	7.84	8.41	1.81	1.16	1.28	3.23

Table 5
Analyses of bulk-rock PGE in part per billion (ppb), Au (ppb), Ni and Cu in part per million (ppm) of chromitites, dunites, harzburgites and lherzolites of the Abdasht ultramafic complex, Iran.

Sample	N-A-4A	N-A-4B	N-A-5A	N-A-5B	N-A-6	N-A-12	N-A-1	N-A-3	N-A-10	N-A-9	N-A-7	N-A-13	N-A-2	N-A-8	N-A-2D
Lithology	Chromite	Chromite	Chromite	Chromite	Chromite	Chr-leopard	Dunite	Dunite	Dunite	Dunite	Harzburgite	Harzburgite	Lherzolite	Lherzolite	Lherzolite
Os	28	22	18	16	60	10	<2	<2	<2	<2	<2	<2	<2	<2	<2
Ir	38	34	34	32	56	21	6	2	<2	3	4	4	3	3	3
Ru	110	103	107	91	136	67	7	7	5	8	6	9	7	6	7
Rh	10	10	17	13	12	7	2	1	<1	1	2	1	1	1	2
Pt	<2	2	<2	<2	<2	<2	4	4	<2	<2	18	10	7	<2	8
Pd	<2	<2	<2	<2	<2	<2	8	<2	<2	<2	7	12	6	9	6
Au	<5	<5	<5	<5	18	5	<5	<5	5	<5	<5	7	<5	7	5
Ni	1070	939	1190	1122	1333	1393	2370	2500	2583	2489	2156	2068	2117	2181	2100
Cu	15	32	19	13	39	6	3	4	4	6	23	21	19	16	19
Total PGE	186	171	176	152	264	105	27	14	5	12	37	36	24	19	26
IPGE	176	159	159	139	252	98	14	10	7	12	11	14	11	10	11
PPGE	12	13	20	15	14	9	14	6	3	3	27	23	14	11	16
ΣIPGE/ΣPPGE	14.67	12.23	7.95	9.27	18.00	10.89	1.00	1.67	2.33	4.00	0.41	0.61	0.79	0.91	0.69
ΣPPGE/ΣIPGE	0.07	0.08	0.13	0.11	0.06	0.09	1.00	0.60	0.43	0.25	2.45	1.64	1.27	1.10	1.45
Pt/Pt*	0.10	0.20	0.08	0.09	0.09	0.12	0.32	0.91	1.28	1.54	0.11	0.32	0.45	0.92	0.74
Pd/Ir	<0.05	<0.06	<0.06	<0.06	<0.04	<0.1	1.33	0.50	*	0.33	1.75	3.00	2.00	3.00	2.00
Cu/Ni	0.01	0.03	0.02	0.01	0.03	0.00	0.00	0.00	0.00	0.00	0.01	0.01	0.01	0.01	0.01
Cu/Ir	395	941	559	406	696	286	500	2000	4000	2000	5750	5250	6333	5333	6333
Ni/Pd	>535,000	>469,500	>595,000	>561,000	>666,500	>696,500	296,250	2,500,000	2,583,000	2,489,000	308,000	172,333	352,833	242,333	350,000
Cu/Pd	>7500	>16,000	>9500	>6500	>19,500	>3000	375	4000	4000	6000	3286	1750	3167	1778	3167
$\Sigma PPGE_N/\Sigma IPGE_N$	0.19	0.21	0.35	0.31	0.15	0.25	1.24	0.69	0.49	0.41	2.26	1.65	1.31	1.40	1.65
$\Sigma IPGE_N/\Sigma PPGE_N$	5.30	4.67	2.84	3.23	6.54	4.05	0.80	1.46	2.06	2.42	0.44	0.60	0.77	0.71	0.61
XRu	0.56	0.59	0.61	0.59	0.47	0.62									
XOs	0.19	0.17	0.14	0.14	0.28	0.13									
XIr	0.25	0.25	0.25	0.27	0.25	0.25									

$Pt/Pt^* = Pt$ anomaly is calculated as $Pt/Pt^* = (Pt/8.3)/\sqrt{[(Rh/1.6) \times (Pd/4.4)]}$. The Pt anomaly ($Pt/Pt^*$), Pd/Ir and $PPGE_N/IPGE_N$ calculated according to half values which were used for statistical calculations of samples with values below detection limit.

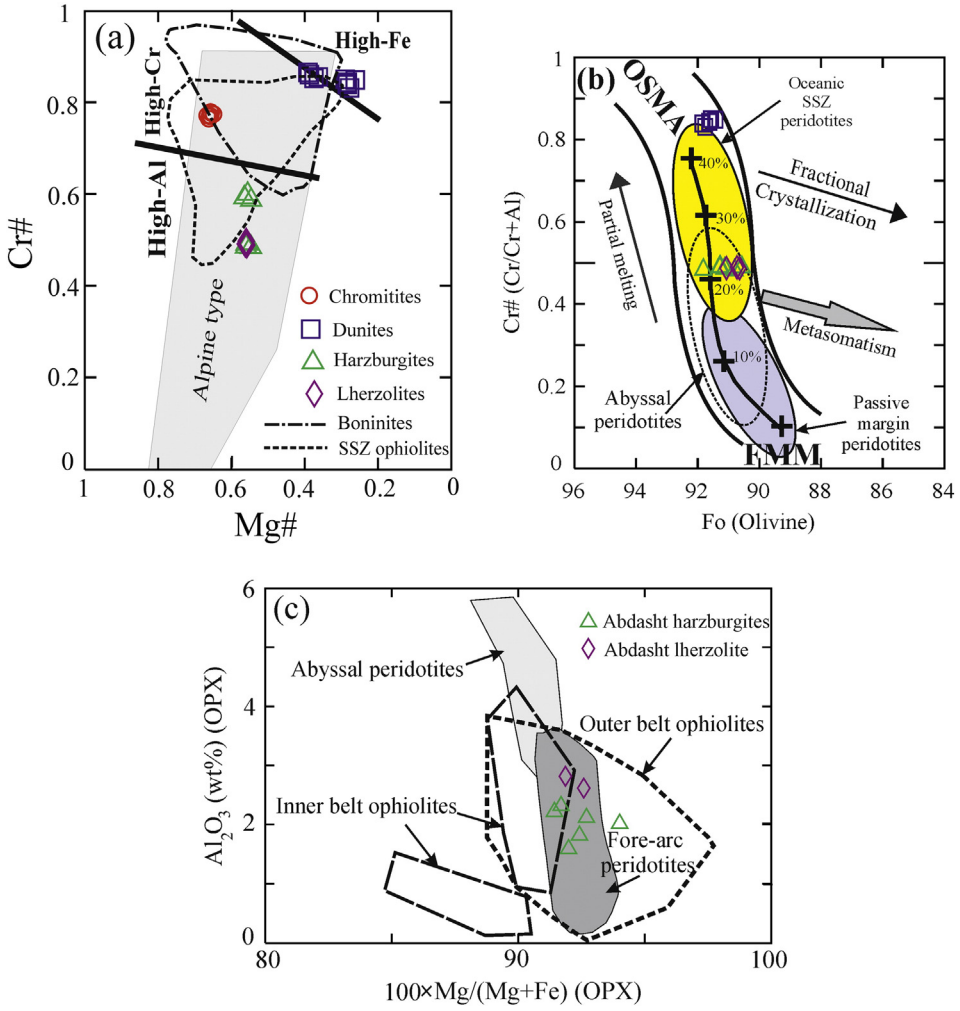

Fig. 5. Variation diagrams showing mineral compositions from the Abdasht ultramafic complex. a) Plot of Cr# vs. Mg# for chromian spinel in chromitite, dunite, harzburgite and lherzolite. The Alpine-type field is from Irvine (1967), supra-subduction zone (SSZ) and boninite fields are from Bridges et al. (1995). Note the distinct groupings into high-A1, high-Cr and high-Fe chromian spinel varieties from Zhou and Bai (1992). b) Chemical variation of Cr-ratio versus Fo content of the olivine-Cr-spinel pairs of the studied harzburgites and dunites. Olivine-spinel mantle array (OSMA), melting trends and amounts of melting are from Arai (1994). The abyssal, fore-arc and passive margin peridotites are from Dick and Bullen (1984); Ishi et al. (1992); Parkinson and Pearce (1998); Pearce et al. (2000) and Choi et al. (2008). c) Diagram showing the variation in Al_2O_3 (wt.%) vs. Mg# of orthopyroxenes from the harzburgite and lherzolite rock varieties. Fore-arc peridotite fields are from Ishi et al. (1992); abyssal peridotite fields are from Johnson et al. (1990). (For interpretation of the references to color in this figure legend, the reader is referred to the web version of this article.)

versus FeO. The Fe^{3+}# [$Fe^{3+}/(Fe^{3+} + Al + Cr)$ atomic ratio] is <0.02 (Table 1). The low Fe^{3+}# values are <0.1. The composition of the chromian spinels reflect crystallization under low oxygen fugacities (Fisk and Bence, 1980) (Tables 1 and 2).

The Cr_2O_3 content varies from 38.4 up to 46.6 wt.%, with an average of 40.9 wt.% in harzburgites, and from 52 up to 59.3 wt.%, with an average of 55 wt % in dunites, and varies in a narrow range from 38.5 up to 39.2 wt.%, with an average of 38.8 wt.% in lherzolites. Dunites of the Abdasht complex are characterized by the very high Cr# (>0.83) of spinel. The Cr# varies from 0.83 up to 0.86 in dunites, from 0.48 up to 0.60 in harzburgites and from 0.49 up to 0.50 in lherzolites (Fig. 5a). The Mg# contents are much lower in dunites than in harzburgites and lherzolites and vary across a wide range from 0.26 up to 0.39 (average 0.32) in dunites, from 0.55 up to 0.57 (average 0.56) in harzburgites and 0.56 in lherzolites (Fig. 5a). The Mg# of spinel in peridotites is empirically related with the grain size of spinel and the Mg# of spinel cores decreases strongly with a decrease in size (Okamura et al., 2006). Chromian spinels in harzburgites and lherzolites exhibit a high-Al composition, whereas grains from the dunites exhibit a high-Fe composition (Fig. 5a). The Al_2O_3 and MgO contents are much lower in dunites than in harzburgites and lherzolites and vary respectively from 6.2 up to 7.1 wt.% (average 6.6 wt.%) and from 5.2 up to 8.1 wt.% (average 6.5 wt.%) (Table 2). The Al_2O_3 and MgO contents vary respectively from 19.8 up to 27.8 wt.% (average 25.2 wt.%) and from 11.4 up to 12.3 wt.% (average 11.9 wt.%) in harzburgites, and from 26.5 up to 27.5 wt.% (average 27 wt.%) and from 12 up to 12.4 wt.% (average 12.3 wt.%) in lherzolites. The FeO content is much higher in dunites than in harzburgites and lherzolites; it ranges from 22.2 up to 26.1 wt.% (average 24.2 wt.%) in dunites, and from 16.3 up to 17.9 wt.% (average 17 wt.%) in harzburgites, and from 16.9 up to 17.5 wt.% (average 17.2 wt.%) in lherzolites (Table 2). The TiO_2 content is low in chromian spinel from the majority of the studied peridotites (≤0.14 wt.%), however some dunite samples may contain chromian spinel with higher TiO_2 abundances. Furthermore, the Fe^{3+}# [$Fe^{3+}/(Fe^{3+} + Cr + Al)$] in chromian spinel is relatively low in most of the peridotites, although chromian spinel in dunite rocks is characterized by somewhat higher Fe^{3+}# values (Table 2).

6.1.2. Olivine, orthopyroxene and clinopyroxene compositions

Olivine has Fo values ranging from 91.3–91.9 in dunites, 90.6–91.8 in harzburgites and 90.7–91.1 in lherzolites (Fig. 5b). The NiO content of olivine in the dunites ranges from 0.31–0.39 wt.% (with an average of 0.34 wt.%), in harzburgites from 0.35–0.40 wt.% (with an average of 0.38 wt.%) and in lherzolites from 0.23–0.30 wt.% (with an average of 0.27 wt.%). The NiO content of olivine in all the examined peridotite types is lower than 0.40 wt.%, which is quite normal for mantle olivine (Ishimaru and Arai, 2008). The olivines in the Abdasht dunites and harzburgites have TiO_2, Al_2O_3 and CaO, but Cr_2O_3 contents below the determination limit of 0.05 wt.% (Table 3).

Orthopyroxene in harzburgite is enstatite ($En_{90.76–93.34}Wo_{0.67–0.74}$) with Mg# of 0.91–0.94 (Fig. 5c). It is also characterized by low Al_2O_3 (≤2.20 wt.%), CaO (≤0.39 wt.%), TiO_2 (≤0.03 wt.%), Cr_2O_3 (≤0.61 wt.%) and K_2O (≤0.01 wt.%), which are similar to composition in depleted harzburgites elsewhere (e.g. Ahmed, 2013; Kapsiotis, 2014). Orthopyroxene in lherzolite is enstatite ($En_{90.46–91.49}Wo_{1.13–1.18}$) with a Mg# of 0.91–0.93, Cr_2O_3 ranging from 0.50 to 0.51 wt.% and low TiO_2 content (<0.04 wt.%). The Al_2O_3, CaO and Cr_2O_3 abundance in orthopyroxene generally increases as the peridotites become more mafic (Table 4).

The Mg# of clinopyroxene in the lherzolites ranges between 0.94 and 0.98, and Cr_2O_3 contents between 0.45 and 0.70 wt.%. All clinopyroxene grains are diopsidic ($En_{47.94–50.33}Wo_{48.53–49.67}$) in composition and have low Al_2O_3 contents (2.68–3.70 wt.%). Na_2O and K_2O were detected in very low abundances (≤0.13 and below detection limit respectively), which is indicative of the residual origin of the analyzed clinopyroxene grains and the strongly depleted character of their host rocks (Table 4). The TiO_2 content in clinopyroxene does not exceed 0.32 wt.%.

6.2. Bulk rock PGE geochemistry in chromitites and associated rocks

Analyses of whole rock major and trace elements and REE concentrations in the peridotites have been presented elsewhere (Ahmadipour, 2000; Najafzadeh and Ahmadipour, 2014b). The vast majority of the studied peridotites are strongly depleted in REE. Therefore, presently only platinum-group elements analyses from chromitites and peridotites of the study area will be used to establish petrogenesis.

Six chromitite samples of different ore bodies and nine peridotite samples were analyzed for PGE (Os, Ir, Ru, Rh, Pt, and Pd), Au, Ni and Cu (Table 5). The PGE concentration in chromitites show narrow variations: 10–60 ppb Os, 21–56 ppb Ir, 67–136 ppb Ru, 7–17 ppb Rh, while Pt and Pd are under detection limit. The chromitites display low to moderate total PGE abundances, ranging between 105 to 264 ppb, with an average of 176 ppb which are typical for the ophiolitic chromitites (100–500 ppb; Leblanc, 1991).

The chromitites are enriched in the Ir-group (IPGE: Os, Ir and Ru) (98–252 ppb) and extremely depleted in the Pt-group (PPGE: Rh, Pt and Pd) (<20 ppb) (ΣIPGE/ΣPPGE = 8–18). Most Pt and Pd contents are below detection limit (<2 ppb) (Fig. 6a) and hence, for all peridotites half values of detection limit for all platinum group elements were used in calculating of some parameters (e.g. Pd_N/Ir_N) similar to some papers (e.g. Pašava et al., 2004) (Table 5). The relative enrichment of IPGE in chromitite samples is also reflected by highly negative slopes from Ru to Pt. These patterns and the low PGE abundances are typical of chromitites in ophiolites from elsewhere (e.g. Ahmed and Arai, 2002; Ahmed et al., 2009; Ahmed and Habtoor, 2015; Chen and Xia, 2008; Ismail et al., 2010; Proenza et al., 2007; Uysal et al., 2009) (Fig. 6a). The IPGE is dominated by Ru (X_{Ru} = Ru/(Os + Ir + Ru) = 0.47–0.62; X_{Os} = Os/(Os + Ir + Ru) = 0.13–0.28; X_{Ir} = Ir/(Os + Ir + Ru) = 0.25–0.27), which are also typical of ophiolitic chromitite deposits (e.g. Vourinos, Newfoundland, Troodos, Luobusa ultra-high pressure chromitites) (Fig. 6a) and have been attributed to the coexistence of alloys and sulfides of laurite type inclusions in chromite (Büchl et al., 2004; Grammatikopoulos et al., 2011). The average Ni content of the chromitites is 1175 ppm, and Cu content is 21 ppm. Except for two samples 5 and 18 ppm), the Au contents are below detection limit (Table 5). According to Jannessary et al. (2012), chromian spinels from Abdasht complex have primitive compositions with low Re/Os (0.013) and chondritic $^{187}Os/^{188}Os$ (0.1275).

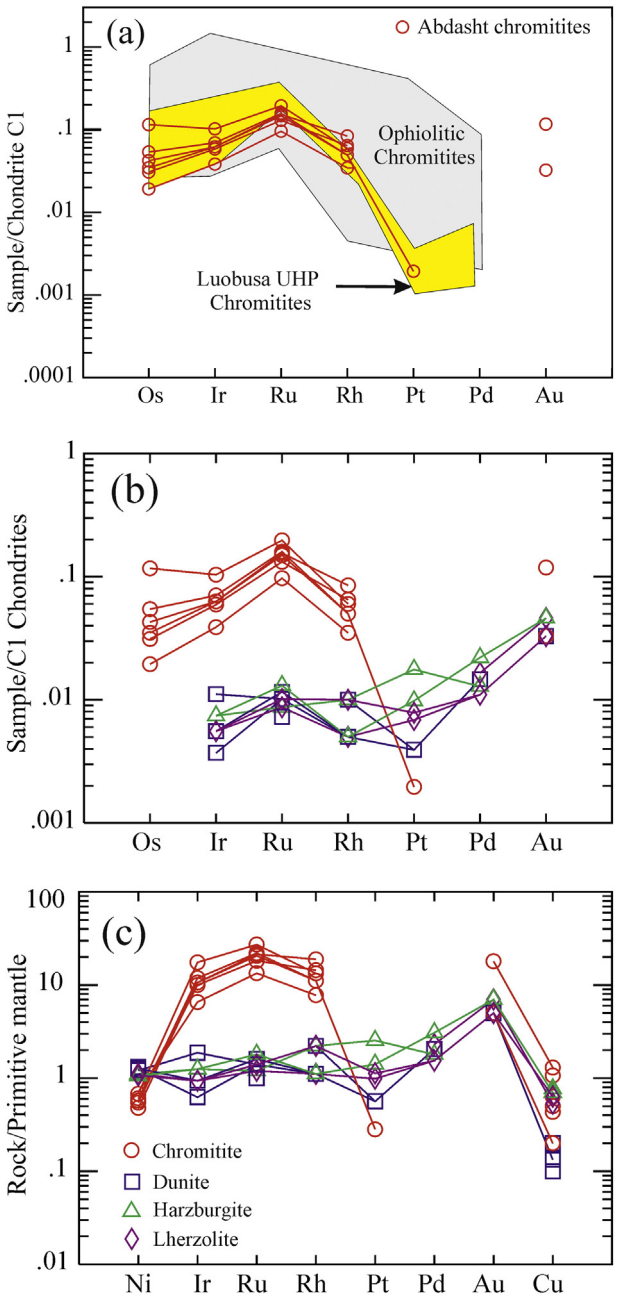

Fig. 6. PGE spidergrams (normalized in whole rock) from the Abdasht ultramafic complex. a) Chondrite normalized PGE patterns for podiform chromitites (red circles). The fields of Luobusa ultra-high pressure (UHP) (Zhou et al., 1996) and ophiolitic chromitite pattern (Kojonen et al., 2003) are used for comparison. Normalizing values currently in use are taken from Naldrett and Duke (1980) (cf. 514, 540, 690, 200, 1020 and 545 for Os, Ir, Ru, Rh, Pt and Pd). b) Chondrite normalized PGE and Au patterns for dunites, harzburgites and lherzolites. c) Primitive mantle normalized plots of chalcophile elements (PGE, Cu, Ni) and Au patterns for dunites, harzburgites and lherzolites. The podiform chromitites are used here for comparison. Chondrite normalization values are from Naldrett and Duke (1980). Mantle normalization values are from McDonough and Sun (1995). (For interpretation of the references to color in this figure legend, the reader is referred to the web version of this article.)

Among the host peridotites of Abdasht complex, the PGE contents of the dunites vary between 5 and 27 ppb, and average 14.5 ppb, and are in

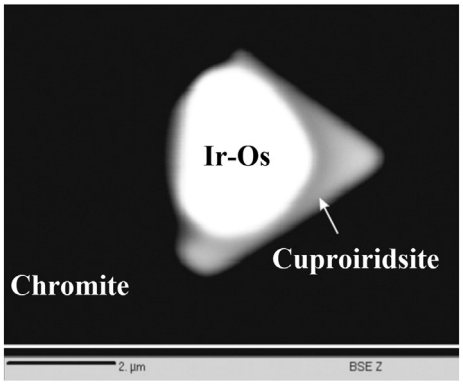

Fig. 7. Two phase inclusion in chromite; cuproiridsite rims an Ir–Os alloy phase, polished section 7507b, level 1, Abdasht Mine (after Jannessary et al., 2012).

agreement with the average content (14.7 ppb) in dunites from other ophiolites. The PGE contents of the harzburgite range from 36 to 37 ppb, are slightly higher than the average value (<30 ppb) in harzburgites from other ophiolites (Shen-Su, 1982). The PGE contents of the Abdasht lherzolites vary from 19 to 26 ppb, with an average of 23 ppb (Table 5).

The PGE spidergrams for dunites show slightly Ru positive anomalies (Fig. 6b,c) and Pt contents in dunites are considerably much lower than those in harzburgites and lherzolites. The Pd_N/Ir_N ratios (Chondrite normalized) in dunites, which considered as index of fractionation, are unfractionated (0.33–1.33) and is slightly higher than the average value (0.12) (Shen-Su, 1982). The harzburgites show slightly positive slopes PGE spidergrams, together with a small positive Ru, Pt and Pd anomalies (Fig. 6b,c), and their Pd_N/Ir_N ratio ranges between 1.75–3 which are higher than the average value (1.08) (Shen-Su, 1982). The lherzolites similarly to dunites show slightly positive slopes PGE spidergrams, together with a small positive Ru and Pd anomaly, and their Pd_N/Ir_N ratio ranges between 2 and 3, but show a few depletion in Ir and Rh relative to harzburgites (Fig. 6b,c). In the mantle normalized Ni, PGE, Au and Cu diagram, the dunites are depleted in Cu relative to harzburgites and lherzolites (Fig. 6c).

6.3. Previous work on the PGM content of the Abdasht chromitites

The only description of PGM from the chromitites of the Abdasht complex was made by Jannessary et al. (2012). Six polished sections of chromitite and associated dunite in Abdasht complex were investigated by reflected light microscopy to characterize the carriers of PGE mineralization and totally 10 PGM ranging in size up to 40 µm were identified.

In a comparative study of high-Cr chromite deposits from the Abdasht complex, it was shown that the PGMs are dominantly IPGE-enriched. The PGM from Abdasht are dominated by Ru-based minerals, mainly represented by laurite (RuS2), cuproiridsite, Ir–Rh sulpharsenides, followed by Ru–Os–Ni–Ir alloys, irarsite, erlichmanite and hollingworthite constitute minor phases. This is in agreement with what is typically found (Os-Ir alloys and laurite–erlichmanite) in mantle hosted ophiolitic chromitites.

Laurite usually forms euhedral crystals from less than 1 to 20 µm in size, and is commonly intergrown with other PGM, BMS, and/or silicates occurring in chromian spinel, but rarely in silicate matrix. The chemical composition of laurite is dominated by the Ru–Os substitution with minor Ir, Rh, Fe, Ni, Cu, Co and As. Irarsite [IrAsS] and hollingworthite [RhAsS] are invariably included in silicates (chlorite, serpentine) or associated with chromite/ferritchromite–silicate contacts and only one laurite included in fresh chromite was found associated with irarsite in a sample from Abdasht ultramafic complex.

In the chromitite samples investigated, primary Os–Ir–Ru-rich alloy phases are rare. Most Os–Ir-rich phases form very small grains (<5 µm) intergrown with laurite, and thus are difficult to analyze by microprobe. (Fig. 7). However, the analyses demonstrate the presence of ruthenium, osmium, and iridium. In a polyphase inclusion with laurite and iridian millerite (AS7499, Abdasht), a phase of approximate composition Ir50Ni25Fe25 was identified probably an intermetallic phase of the garutiite (Ni, Ir, Fe) –hexaferrum (Fe, Os, Ru, Ir) solid solution series (McDonald et al., 2010). Pt–Fe alloy phases are rare in Abdasht complex.

The chromitites carrying PGE mineralization in the Abdasht complex are sulfide-poor. Pentlandite is the major constituent of base metal sulfide mineralization in chromitite and dunite of the Abdasht complex, forming small inclusions within chromian spinel and occasionally in olivine. In some chromitites, pentlandite forms euhedral grains interstitial to both, unaltered chromian spinel and olivine. Pentlandite is frequently intergrown with a Cu-rich sulfide phase, either with chalcopyrite, cubanite or chalcocite in interstitial aggregates, or with bornite and chalcopyrite in inclusions (Jannessary et al., 2012).

7. Discussion

7.1. Parental melt composition of chromitites

Experimental work has demonstrated that chromian spinel and olivine are sensitive petrogenetic indicators and used to constrain the chemistry of parental melt (e.g. Arai, 1992; Dick and Bullen, 1984; Irvine, 1967; Melcher et al., 1997; Zhou et al., 1996; Zhou et al., 2005).

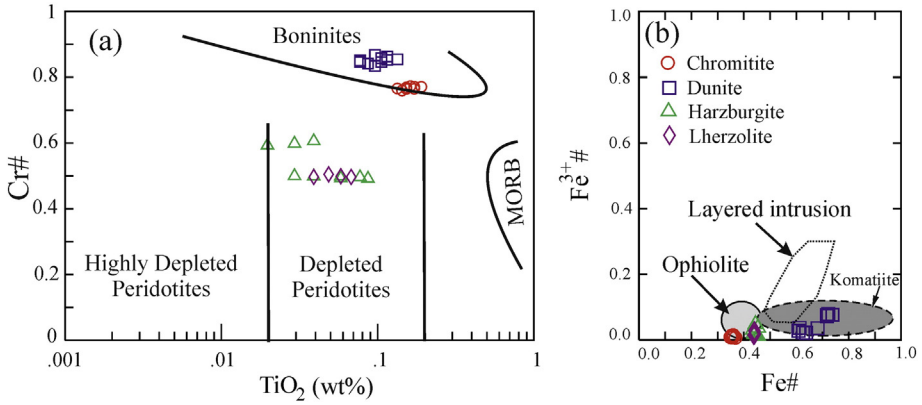

Fig. 8. a) TiO_2 versus Cr# in chromian spinels, showing fields of boninites and MORB (mid-ocean ridge basalts) (after Arai, 1992; Dick and Bullen, 1984). Fields of depleted and highly depleted peridotites are from Jan and Windley (1990). Chromian spinels of the Abdasht chromitites and dunites plot in the boninitic field whereas those of harzburgites and lherzolites plot in the depleted peridotites field. b) Fe^{3+}# as a function of Fe^{2+}#. Fields of ophiolites, layered intrusions and komatiites are from Barnes and Roeder (2001).

Chromitites plot in the boninitic field and are clearly distinct from the MORB types in the plots of Cr# versus Mg# (Fig. 5a) and Cr# versus TiO_2 wt.% (Fig. 8a). On the other hand, the low Fe^{3+}#[$=Fe^{3+}/(Fe^{3+}+Cr+Al)$ value < 0.1] (Table 2) (Fig. 8b) reflect crystallization under lower oxygen fugacity (Fisk and Bence, 1980).

The Al_2O_3 contents of the melt can be calculated from the Maurel and Maurel (1982) formula:

$$Al_2O_3 wt.\%_{chromite} = 0.035\ (Al_2O_3)^{2.42} wt.\%_{liquid}$$

The model results derived from this equation are not sensitive to temperature, so it can be used to compute the Al_2O_3 content of the Abdasht melt. The results show that Al_2O_3 contents of the liquids for the most chromitites ranging from 11.2 to 11.5 wt.%. These values are similar to the boninitic melts reported from e.g., the Troodos ophiolite in Cyprus (Robinson et al., 1983); Luobusa ophiolite in Southern Tibet (Zhou et al., 1996), and Cr-rich chromitites from Nidar ophiolite in Trans Himalaya (Ravikant et al., 2004).

Kamenetsky et al. (2001) have shown, using melt inclusions in chromian spinel from volcanic rocks, that there is a linear relationship between the Al_2O_3 and TiO_2 contents of chromian spinel and the melt from which it crystallized.

Rollinson (2008), building on the earlier observations of Kamenetsky et al. (2001) and Wasylenki et al. (2003), show that the Al_2O_3 and TiO_2 contents of chromian spinel correlate with those of the melt. The TiO_2 content of the melt can be determined from the melt-TiO_2 versus spinel-TiO_2 regression lines using the data of Kamenetsky et al. (2001). Applying the approach of Rollinson (2008), we have calculated the Al_2O_3 and TiO_2 contents of the melt in equilibrium with chromitites from the Abdasht complex and results are shown in Table 1 and represented graphically in Fig. 9. The TiO_2 contents of the parental melt of Abdasht chromitites vary between 0.23 to 0.31 wt.% (average 0.27 wt.%), which indicates a boninitic-type parental melt.

The FeO/MgO ratio of the melt in chromitites has been calculated using the formula of Maurel (1984; cited in Augé, 1987) (Table 1). The melts that produced the chromian spinel of the Abdasht chromitites contained 11.92–12.25 wt.% Al_2O_3, with FeO/MgO ratios varying between 0.60 and 0.65 (Table 1). The compositions of the melts parental to the chromian spinel of the Abdasht chromitites resemble the boninites of Bonin Island, Japan (e.g. Hickey and Frey, 1982). Similar melts of boninitic affinity have been suggested to be responsible for the formation of high-Cr chromitites from many localities such as Kempirsai in Kazakhstan (Melcher et al., 1997), Muğla in Turkey (Uysal et al., 2009), Elekdag ophiolite in Turkey (Dönmez et al., 2014), Nidar ophiolite chromitites (Ravikant et al., 2004), Mayari-Cristal ophiolitic massif in eastern Cuba (González-Jiménez et al., 2011) and Sorkhband, Soghan and Dehsheikh ultramafic complex in Iran (Najafzadeh et al., 2008; Najafzadeh and Ahmadipour, 2014a; Peighambari et al., 2015) (Table 6). Parental melts to Oman and Thailand chromitites (Orberger et al., 1995; Rollinson, 2008) have similar FeO/MgO (average 0 · 63) and a few lower Al_2O_3 (>11 · 4 wt.%) than Abdasht chromitites. Calculated compositions of melts from which Abdasht chromitites formed are similar to high-MgO boninites (Table 6).

Fig. 10 a and b show the calculated TiO_2 and Al_2O_3 contents of the parental melt of the Abdasht chromitite. The compositions of the chromian spinel in chromitites are indicative of crystallization from melts derived from depleted mantle. Chromitite samples from the Abdasht complex have low TiO_2 and Al_2O_3 contents plot away from the MORB field but show strong affinity with melts from depleted mantle and boninites (Fig. 10a) similar to Oman (Ishikawa et al., 2002), Troodos (Cameron, 1985; Flower and Levine, 1987), Thetford boninites (Pagé and Barnes, 2009), and Elekdağ high-Cr chromitites (Dönmez et al., 2014) (Fig. 10b). The Cu/Ir versus Ni/Pd diagram (Fig. 10c) of the peridotites point to similar conclusions.

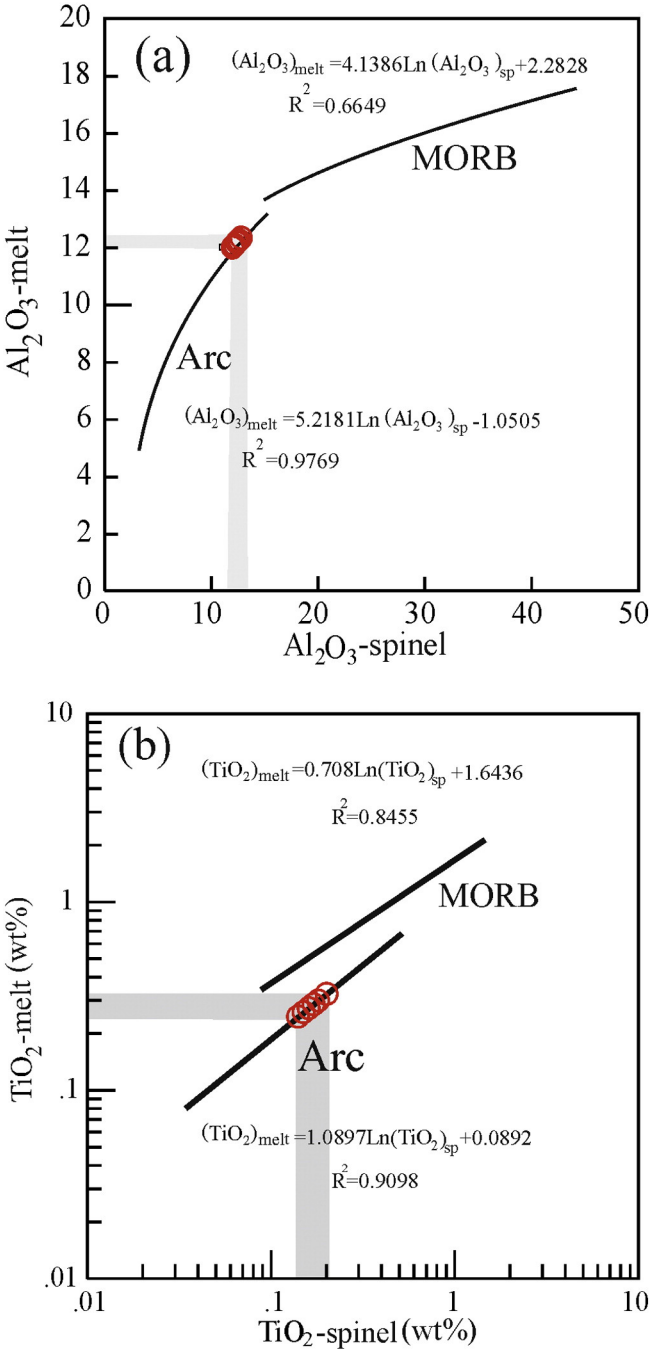

Fig. 9. Al_2O_3 a) and TiO_2 b) contents of the melt in equilibrium with chromitites from the Abdasht complex, using data on chromite-melt inclusions in MORB and arc lavas reported by Kamenetsky et al. (2001) and Rollinson (2008). The range of chromian spinel and the calculated melt compositions from the Abdasht complex are shown as gray fields.

7.2. Distribution, concentration and fractionation of PGE in chromitites and associated rocks

Ophiolitic chromitites worldwide show variable PGE contents, commonly less than 500 ppb, and Pd_N/Ir_N ratios between 0.8–0.1, although in some instances they may contain higher total PGE (>750 ppb) and display very low Pd_N/Ir_N ratios (<0.1) (e.g. Ahmed and Arai, 2002; Gervilla et al., 2005; Leblanc, 1991; Zhou et al., 1998). Cr and PGE, beneath the mid-ocean ridge setting, generally behave compatibly during dry partial melting in the upper mantle (Büchl et al., 2004; Dick and

Table 6
Comparison between parental melt composition of Abdasht chromitites and other worldwide high-Cr podiform chromitites. Computations of Al_2O_3 and TiO_2 were made using the approaching of Kamenetsky et al. (2001) and Rollinson (2008), whereas FeO/MgO calculations are according to Maurel and Maurel (1982).

	Cr#	Al_2O_3 (spinel)	Al_2O_3 (melt)	TiO_2 (spinel)	TiO_2 (melt)	FeO/MgO(melt)	Reference
Abdasht chromitites (Iran)	0.76-0.77	12.00–12.80	11.92–12.25	0.14–0.20	0.23–0.31	0.60–0.65	This study
Dehsheikh chromitites (Iran)	0.68–0.79	10.29–16.90	11.10–14.50	0.12–0.27	0.21–0.49	0.99–1.20	Peighambari et al. (2015)
Soghan chromitites (Iran)	0.80–0.84	8.23–10.23	9.95–11.08	0.10–0.29	0.18–0.41	0.65–0.84	Najafzadeh and Ahmadipour (2014a)
Sorkhband chromitites (Iran)	0.75–0.89	9.32	10.05	0.08		0.70	Najafzadeh et al. (2008)
Muğla chromitites (SW Turkey)	0.64–0.75		8.80–10.50			0.30–1.10	Uysal et al. (2009)
Elekdağ ophiolite (Northern Turkey	0.65–0.89	5.10–18.20	9.40–13.20	0.14–0.26	0.20–0.40	0.40–1.90	Dönmez et al. (2014)
Nan Uttardite chromitites (Thailand)			11.60–12.00				Orberger et al. (1995)
Deep chromitites (Oman)	0.71–0.77	11.70–14.40	11.80–12.90		0.23–0.34		Rollinson (2008)
Massive chromitite (Kempirsai)			9.00–10.60			0.30–0.50	Melcher et al. (1997)
High-Cr chromitites (Eastern Cuba)	0.63–0.72	16.30	13.40	0.19	0.30	0.90–1.50	González-Jiménez et al. (2011)
Boninite			11.29–14.87		0.22–0.24	0.68–0.89	Falloon et al. (2008)
MORB			~14.70			~1.37	Gale et al. (2013)

Bullen, 1984) due to their restricted mobility. In contrast, PGE, especially PPGE, behave incompatibly during hydrous partial melting in a supra-subduction zone setting, where the degree of partial melting is much higher than in a mid-ocean ridge setting.

As stated by many authors (e.g. Ahmed and Arai, 2002; Arai and Matsukage, 1998 and references therein) in supra-subduction zone settings, the mantle wedge has been partially melted severally and the resulted peridotites are highly depleted. This feature has discussed in Abdasht complex by REE depleted nature of these peridotites (Ahmadipour, 2000). But due to the enrichment of depleted mantle wedge by slab derived fluids, peridotites have been metasomatized and then, partial melting event has been done under hydrous conditions. This stage of partial melting will leave behind a podiform chromitite highly depleted in PPGE and notably enriched in Cr and IPGE (e.g. Ahmed and Arai, 2002; Büchl et al., 2004; Grammatikopoulos et al., 2011; Zhou et al., 1998).

The Abdasht chromitites contain up to 264 ppb total PGE, and display a systematic enrichment in IPGE relative to PPGE, with a steep negative slope in the PGE spidergrams and very low PPGE/IPGE ratios, a feature typical of worldwide ophiolitic podiform chromitites (e.g. Ahmed and Arai, 2002; Büchl et al., 2004; González-Jiménez et al., 2011; Leblanc, 1991; Tsoupas and Economou-Eliopoulos, 2008; Zhou et al., 2005) (Fig. 6a). Chromitite and peridotite samples in Abdasht ultramafic complex have a wide range in Pd/Ir values (<0.04 to 0.1 in chromitites and 0.33 to 3 in peridotites) which reflect variations in the amounts of partial melting rather than magmatic fractionation (Fig. 11a). In the plot of Ni/Cu versus Pd/Ir, the Abdasht peridotites lie around the partial melting line, and show that the Pd/Ir ratios were controlled by S-undersaturated melts and partial melting processes (Fig. 11b).

The main hosts of PPGE, i.e. Pd and Pt, in the upper mantle rocks are the base metal sulfides (e.g. Luguet et al., 2003). High-degrees of partial melting and complete dissolution of the sulfides, lead to leaching of PPGE from the peridotites and transferring them into the S-undersaturated magmas (e.g. Zhou et al., 1998), leaving a mantle residue highly depleted in these elements. Strong depletion of PPGE in the Abdasht peridotites coupled with the high Cr# values determined for spinels (>0.80), strongly indicate that either a high-degree of partial melting or partial melting of an already depleted mantle peridotite (second-stage melting) was responsible for the formation of the Abdasht chromitites. These conditions are believed to develop in suprasubduction zone settings similar to the podiform chromitites from Bou Azzer ophiolite in Morroco (Ahmed et al., 2009). This also implies that the Abdasht chromitites have been derived from highly S-undersaturated boninitic magmas which have been able to dissolve the mantle sulfides and partly removed the Pd and Pt resident in their mantle host rocks. This type of melting is formed in the suprasubduction zone environment. The highly refractory nature of the mantle peridotites, the strong decoupling of the PGE subgroups and the small size of the chromitite pods in the Abdasht upper mantle are strong evidence for a second-stage melting model (Ahmed et al., 2009; Zhou et al., 1998).

7.3. Tectonic Setting of chromitites and peridotites from Abdasht complex

The composition of chromian spinel provide valuable evidence on the geochemical signature of the parental magmas and the tectonic setting of their genesis. In this study, the field relationships together with the geochemical characteristics of chromitite and associated ultramafic rocks of the Abdasht complex can be used to constrain the tectonic setting of the Esfandagheh area.

The island-arcs and back-arcs settings are the most widely-accepted settings for the formation of podiform chromitites (e.g. Rollinson, 2008; Uysal et al., 2007; Zhou et al., 1998). In these settings, chromitites form by the interaction of upper mantle lithologies with migrating magmas produced at greater depth (Arai and Yurimoto, 1994; Zhou and Bai, 1994). The TiO_2 content, considered a key factor for the identification of the tectonic setting (e.g. Arai and Matsukage, 1998; Bonavia et al., 1993), is extremely low in the dunite, harzburgite and lherzolite chromian spinels averaging 0.11, 0.05 and 0.06 wt.%, respectively. Kamenetsky et al. (2001) compiled a database of Al_2O_3 and TiO_2 compositions of chromian spinel and identified fields with varying degrees of overlap that can be used to distinguish six different tectonic settings. Thus, chromian spinel compositions from chromitites and peridotites from Abdasht complex plot in the arc and supra-subduction zone fields (Fig. 12a). On the other hand, the diagram TiO_2 versus Fe_2O_3 indicates that almost all samples plot within the field of suprasubduction zone ophiolites (Fig. 12b). In addition, as shown in Fig. 6a, PGE relative proportions from Abdasht chromian spinels follow the trends of ophiolitic chromitites (Fig. 6a).

Variations in the TiO_2 content versus the Al_2O_3 in chromian spinels from the chromitites, dunites, harzburgites and lherzolites suggest that the chromian spinel of both chromitite and peridotites are restricted to supra-subduction zone environments (Fig. 12a) with boninitic affinity. This is in agreement with the calculated FeO/MgO and Al_2O_3 values in parental melt of chromian spinels (Fig. 12c). Because boninites are restricted to fore-arcs in modern tectonic environments, their presence in ancient assemblages is often taken to indicate a fore-arc environment (Coish and Gardner, 2004).

The Abdasht ultramafic complex is a part of Haji Abad-Esfandagheh ophiolites in the outer Zagros ophiolitic belt (Rajabzadeh et al., 2013; Shafaii Moghadam and Stern, 2011). Therefore, it can represent remnants of southern branch of Neo-Tethyan ocean in Iran outcropping in Kerman province south-east of Iran (Fig. 1a). Chemical compositions of Abdasht chromian spinels in harzburgites also confirm a fore-arc setting for the complex, similarly to other ophiolites in the outer Zagros

ophiolitic belt (Fig. 5c). Moreover, variations in the Cr# content versus TiO_2 in chromian spinels from the chromitites, dunites, harzburgites and lherzolites are consistent with the Abdasht complex plot within the field of fore-arc peridotites and boninites (Fig. 12d).

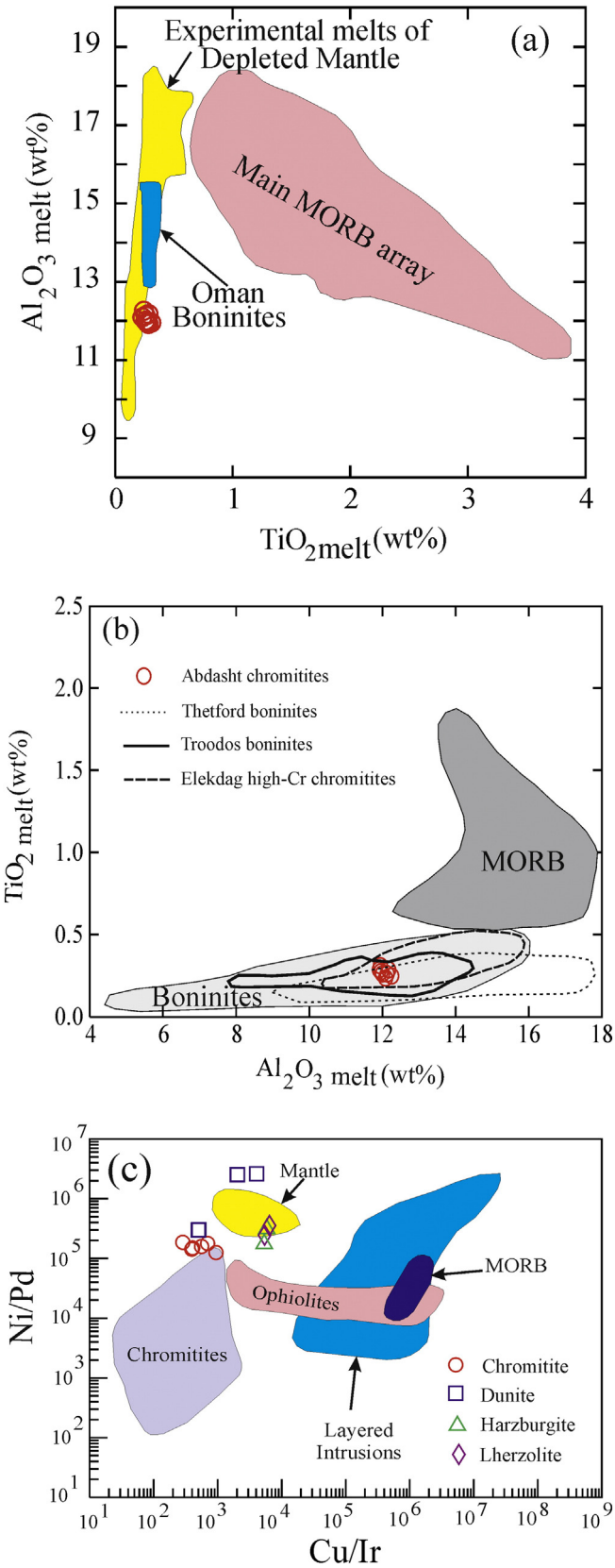

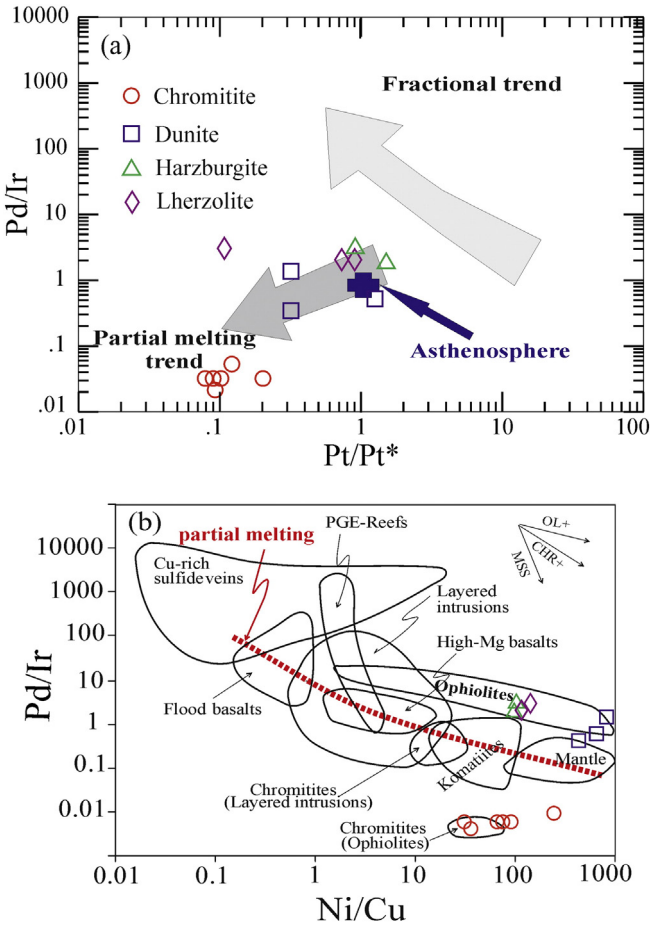

Fig. 11. a) Plot of platinum anomaly (Pt/Pt*) versus Pd/Ir in chromitites and peridotites from the Abdasht complex. Fractionation and partial melting trends are from Garuti et al. (1997). The Pt anomaly is calculated as $Pt/Pt^* = (Pt/8.3)/\sqrt{[(Rh/1.6) \times (Pd/4.4)]}$. (b) Plots of Ni/Cu versus Pd/Ir for the chromitites and peridotites of the Abdasht ultramafic complex. Reference fields are from Barnes et al. (1988).

Abdasht chromitites are high-Cr chromian spinels which are formed from boninitic magmas in fore-arc environments (Fig. 12d). Moreover, evidences such as the existence of high-Cr (podiform) chromitite bearing dunites also suggest a fore-arc setting for the Abdasht ultramafic complex. Boninitic melts, which are abundant in this tectonic setting, could have formed high-Cr chromitite deposits in the Abdasht complex. Spinels have low TiO_2 contents (<0.14 wt.%) and are Cr-rich (Cr# ~ 0.48–0.86) in the Abdasht peridotites (mainly in dunites) and are also similar to spinels from fore-arc peridotites (Fig. 12d) (Ohara, 2006). Boninites are common in nearly all of the Late Cretaceous Neo-Tethyan ophiolites as well as the Zagros Inner and Outer Belt ophiolites. These rocks are essentially found in fore-arc environments such as in the IBM fore-arc region (Shafaii Moghadam et al., 2013).

Fig. 10. a) TiO_2 versus Al_2O_3 plot showing the field of the main MORB array, the diagram and parental melt calculations from Rollinson (2008). Field of the Oman boninites (data from Ishikawa et al., 2002) and melts of depleted mantle (DM) from Schwab and Johnston (2001). b) The TiO_2 and Al_2O_3 (wt.%) content of the melt calculated as in equilibrium with chromian spinel from podiform chromitites in the Abdasht ultramafic complex. Fields for boninites (Jenner, 1981; Kamenetsky et al., 2002; Walker and Cameron, 1983), Troodos boninites (Cameron, 1985; Flower and Levine, 1987), Thetford boninites (Pagé and Barnes, 2009), Elekdağ high-Cr chromitites (Dönmez et al., 2014) and MORB (Le Roex et al., 1987; Presnall and Hoover, 1987; Shibata et al., 1979) are shown for comparison. c) Plots of Cu/Ir versus Ni/Pd for the mantle chromitites and peridotites of the Abdasht complex. Reference fields are from Barnes et al. (1988).

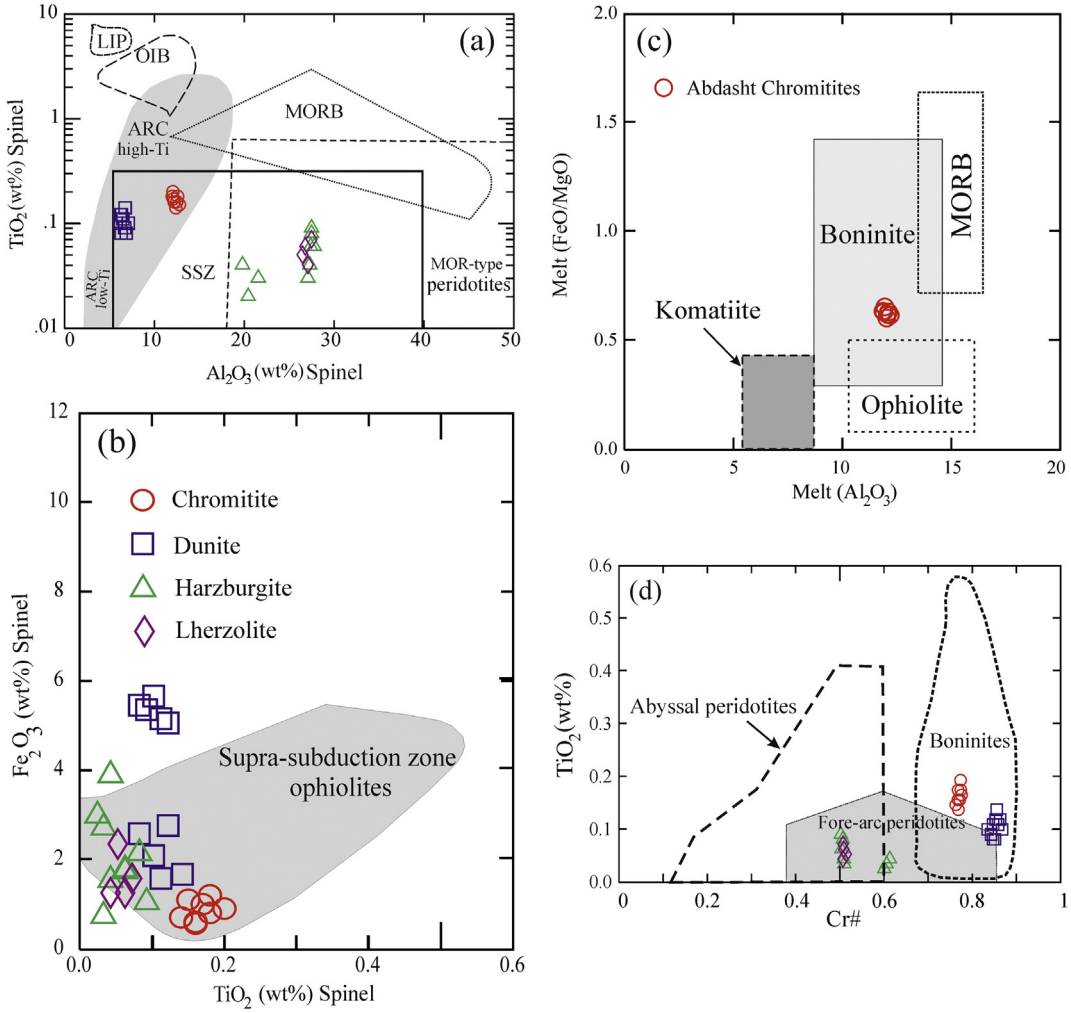

Fig. 12. Tectonic discrimination diagrams. a) Plot of TiO_2 versus Al_2O_3 in chromian spinel from the Abdasht complex with respect to modern-day tectonic settings. The fields are from Kamenetsky et al., 2001). SSZ; Supra-subduction zone; LIP, large igneous province; MORB, mid-ocean ridge basalt; OIB, ocean island basalt. b) Plot of TiO_2 versus Fe_2O_3 of chromian spinels of Abdasht Complex. The field of supra-subduction zone ophiolites from (Bridges et al., 1995). c) Estimated variation of the parental melt composition in terms of FeO/MgO versus Al_2O_3 wt.% in the Abdasht complex. Tectonic compositional fields are from Barnes and Roeder (2001). d) The relation between Cr# and TiO_2 of chromian spinel in podiform chromitites, dunites, harzburgites and lherzolites of the Abdasht complex. Note that most chromian spinels plot in the fields for both fore-arc peridotites and boninites. Discrimination fields are after Tamura and Arai (2006).

8. Concluding remarks

The main conclusions from this study are summarized below:

1-. The Abdasht complex consists of predominantly harzburgite, pockets of dunite, and minor lherzolite with major podiform chromitite ore deposits.
2-. The peridotites represent depleted residues of a mantle protolith after high degree of partial melting as indicated by the low clinopyroxene content, high Cr# in chromian spinel and Mg# in olivine.
3-. In the complex, refractory harzburgites are dominant and dunites host significant Cr-rich chromitite, but the original boundaries between them have been obliterated by faulting.
4-. Chromitites are enriched in IPGE and strongly depleted in PPGE, i.e. very low PPGE/IPGE values, both features are typical of worldwide ophiolitic podiform chromitites. The PGE patterns in the peridotites are flat which are similar to the highly depleted mantle rocks and indicate a high degree of partial melting (20–25%) of the mantle source (Najafzadeh and Ahmadipour, 2014b).
5-. The relatively low PGE contents of the studied chromitites are in agreement with the sulfide undersaturated nature of the parental melt.
6-. Mg rich olivine (Fo_{91-92}) and orthopyroxene (En_{91-93}), very low TiO_2 content of chromian spinel and the Cr-rich spinel compositions of the ultramafics and associated podiform chromitites from Abdasht are consistent with the rocks forming in a supra-subduction zone environment. It possibly has genetic linkage with some fore-arc related magma with boninitic affinity under a low oxygen fugacity conditions which is in agreement with the geodynamic setting proposed for the outer Zagros ophiolitic belt (including Esfandagheh area).

Acknowledgments

We thank the handling guest editor and two anonymous referees for their constructive and helpful comments. The financial support for the Abdasht ultramafic complex studies that came from the Research Council of Payame Noor University (grant number 69604 to ARN) is acknowledged.

References

Ahmadipour, H., 2000. Petrology and geochemistry of Soghan and Abdasht ultramafic-mafic complexes, north-west of Dowlatabad Baft (PhD thesis. 430p.).

Ahmadipour, H., Sabzehei, M., Whitechurch, H., Rastad, E., Emami, M.H., 2003. Soghan complex as an evidence for paleospreading center and mantle diapirism in Sanandaj–Sirjan zone (South-east Iran). J. Sci. Islam. Repub. Iran 14 (2), 157–172.
Ahmed, A.H., 2013. Highly depleted harzburgite–dunite–chromitite complexes from the Neoproterozoic ophiolite, south Eastern Desert, Egypt: a possible recycled upper mantle lithosphere. Precambrian Res. 233, 173–192. http://dx.doi.org/10.1016/j.precamres.2013.05.001.
Ahmed, A.H., Arai, S., 2002. Unexpectedly high PGE chromitite from the deeper mantle section of the northern Oman ophiolite and its tectonic implications. Contrib. Mineral. Petrol. 143, 263–278.
Ahmed, A.H., Arai, S., Abdel-Aziz, Y.M., Ikenne, M., Rahimi, A., 2009. Platinum-group elements distribution and spinel composition in podiform chromitites and associated rocks from the upper mantle section of the Neoproterozoic Bou Azzer ophiolite, Anti-Atlas, Moroco. J. Afr. Earth Sci. 55, 92–104.
Ahmed, A.H., Habtoor, A., 2015. Heterogeneously depleted Precambrian lithosphere deduced from mantle peridotites and associated chromitite deposits of Al'Ays ophiolite, Northwestern Arabian Shield. Saudi Arabia. Ore Geology Reviews. 67, 279–296.
Alavi, M., 2004. Regional stratigraphy of the Zagros fold-thrust belt of Iran and its proforeland evolution. Am. J. Sci. 304, 1–20.
Allahyari, K., Saccani, E., Rahimzadeh, B., Zeda, O., 2014. Mineral chemistry and petrology of highly magnesian ultramafic cumulates from the Sarve-Abad (Sawlava) ophiolites (Kurdistan, NW Iran): new evidence for boninitic magmatism in intra-oceanic fore-arc setting in the Neo-Tethys between Arabia and Iran. J. Asian Earth Sci. 79 (Part A), 312–328.
Arai, S., 1992. Petrology of peridotites as a tool of insight into mantle processes: a review. J. Mineral. Petrol. Econ. Geol. 87, 351–363.
Arai, S., 1994. Characterization of spinel peridotites by olivine-spinel compositional relationships: Review and interpretation. Chemical Geology. 113, 191–204.
Arai, S., Matsukage, K., 1998. Petrology of a chromitite micropod from Hess Deep, equatorial Pacific: a comparison between abyssal and alpine-type podiform chromitites. Lithos 43, 1–14. http://dx.doi.org/10.1016/s0024-4937(98)00003-6.
Arai, S., Yurimoto, H., 1994. Podiform chromitites of the Tari–Misaka ultramafic complex, southwestern Japan, as mantle–melt interaction products. Econ. Geol. 89, 1279–1288. http://dx.doi.org/10.2113/gsecongeo.89.6.1279.
Arai, S., Kadoshima, K., Morishita, T., 2006. Widespread arc-related melting in the mantle section of the northern Oman ophiolite as inferred from detrital chromian spinels. J. Geol. Soc. 163, 869–879. http://dx.doi.org/10.1144/0016-76492005-057.
Augé, T., 1987. Chromite deposits in the northwestern Oman ophiolite: mineralogical constraints. Miner. Deposita 22, 1–10. http://dx.doi.org/10.1007/BF00204235.
Babaie, H.A., Ghazi, A.M., Babaei, A., La Tour, T.E., Hassanipak, A.A., 2001. Geochemistry of arc volcanic rocks of the Zagros Crush Zone, Neyriz, Iran. J. Asian Earth Sci. 19, 61–76. http://dx.doi.org/10.1016/S1367-9120(00)00012-2.
Barnes, S.-J., Roeder, P.L., 2001. The range of spinel compositions in terrestrial mafic and ultramafic rocks. J. Petrol. 42, 2279–2302. http://dx.doi.org/10.1093/petrology/42.12.2279.
Barnes, S.-J., Boyd, R., Korneliussen, A., Nilsson, L.P., Often, M., Pedersen, R.B., et al., 1988. The Use of Mantle Normalization and Metal Ratios in Discriminating Between the Effects of Partial Melting, Crystal Fractionation and Sulphide Segregation on Platinum-Group Elements, Gold, Nickel, and Copper: Examples from Norway. In: Prichard, H.M., Potts, P.J., Bowles, J.F.W., Cribb, S.J. (Eds.), Geo-Platinum 87. Elsevier, pp. 113–143.
Berberian, M., King, G.C.P., 1981. Towards a paleogeography and tectonic evolution of Iran. Can. J. Earth Sci. 18, 210–265. http://dx.doi.org/10.1139/e81–019.
Bonatti, E., Michael, P.J., 1989. Mantle peridotites from continental rifts to ocean basins to subduction zones. Earth Planet. Sci. Lett. 91, 297–311. http://dx.doi.org/10.1016/0012-821x(89)90005-8.
Bonavia, F.F., Diella, V., Ferrario, A., 1993. Precambrian podiform chromitites from Kenticha Hill, southern Ethiopia. Econ. Geol. 88, 198–202. http://dx.doi.org/10.2113/gsecongeo.88.1.198.
Bridges, J.C., Prichard, H.M., Meireles, C.A., 1995. Podiform chromitite-bearing ultrabasic rocks from the Braganca massif, northern Portugal: fragments of island arc mantle? Geol. Mag. 132, 39–49.
Büchl, A., Brügmann, G., Batanova, V.G., 2004. Formation of podiform chromitite deposits: implications from PGE abundances and Os isotopic compositions of chromites from the Troodos complex, Cyprus. Chem. Geol. 208, 217–232. http://dx.doi.org/10.1016/j.chemgeo.2004.04.013.
Cameron, W.E., 1985. Petrology and origin of primitive lavas from the Troodos ophiolite, Cyprus. Contrib. Mineral. Petrol. 89, 239–255. http://dx.doi.org/10.1007/bf00379457.
Caran, Ş., Çoban, H., Flower, M.F.J., Ottley, C.J., Yılmaz, K., 2010. Podiform chromitites and mantle peridotites of the Antalya ophiolite, Isparta Angle (SW Turkey): implications for partial melting and melt–rock interaction in oceanic and subduction-related settings. Lithos 114, 307–326. http://dx.doi.org/10.1016/j.lithos.2009.09.006.
Chen, G., Xia, B., 2008. Platinum-group elemental geochemistry of mafic and ultramafic rocks from the Xigaze ophiolite, southern Tibet. J. Asian Earth Sci. 32, 406–422. http://dx.doi.org/10.1016/j.jseaes.2007.11.009.
Choi, S.H., Shervais, J.W., Mukasa, S.B., 2008. Supra-subduction and abyssal mantle peridotites of the coast range ophiolite, California. Contrib. Mineral. Petrol. 156, 551–576.
Coish, R.A., Gardner, P., 2004. Suprasubduction-zone peridotite in the northern USA Appalachians: evidence from mineral composition. Mineral. Mag. 68, 699–708. http://dx.doi.org/10.1180/0026461046840214.
Dare, S.A.S., Pearce, J.A., McDonald, I., Styles, M.T., 2009. Tectonic discrimination of peridotites using fO2–Cr# and Ga–Ti–FeIII systematics in chrome–spinel. Chem. Geol. 261, 199–216. http://dx.doi.org/10.1016/j.chemgeo.2008.08.002.
Dick, H.J.B., Bullen, T., 1984. Chromian spinel as a petrogenetic indicator in abyssal and Alpine peridotite and spatially associated lavas. Contrib. Mineral. Petrol. 86, 54–76.
Dilek, Y., Furnes, H., Shallo, M., 2007. Suprasubduction zone ophiolite formation along the periphery of Mesozoic Gondwana. Gondwana Res. 11, 453–475. http://dx.doi.org/10.1016/j.gr.2007.01.005.
Dönmez, C., Keskin, S., Günay, K., Çolakoğlu, A.O., Çiftçi, Y., Uysal, İ., et al., 2014. Chromite and PGE geochemistry of the Elekdağ Ophiolite (Kastamonu, Northern Turkey): Implications for deep magmatic processes in a supra-subduction zone setting. Ore Geol. Rev. 57, 216–228. http://dx.doi.org/10.1016/j.oregeorev.2013.09.019.
Droop, G.T.R., 1987. A general equation for estimating Fe^{3+} concentrations in ferromagnesian silicates and oxides from microprobe analyses using stoichiometric criteria. Mineral. Mag. 51, 431–435.
Falloon, T.j., Danyushevsky, L.V., Crawford, A.J., Meffre, S., Woodhead, J.D., Bloomer, S.H., 2008. Boninites and adakites from the northern termination of the Tonga trench: implications for adakite petrogenesis. J. Petrol. 49, 697–715.
Fisk, M.R., Bence, A.E., 1980. Experimental crystallization of chrome spinel in FAMUS basalt 527–1-1. Earth Planet. Sci. Lett. 48, 111–123.
Flower, M.J., Levine, H., 1987. Petrogenesis of a tholeiite-boninite sequence from Ayios Mamas, Troodos ophiolite: evidence for splitting of a volcanic arc? Contrib. Mineral. Petrol. 97, 509–524. http://dx.doi.org/10.1007/bf00375328.
Gale, A., Dalton, A.D., Langmuir, C.H., Su, Y., Schilling, J.-G., 2013. The mean composition of ocean ridge basalts. Geochem. Geophys. Geosyst. 14, 489–518.
Garuti, G., Fershtater, G., Bea, F., Montero, P., Pushkarev, E.V., Zaccarini, F., 1997. Platinum group elements as petrological indicators in mafic–ultramafic complexes of the central and southern Urals: preliminary results. Tectonophysics 276, 181–194. http://dx.doi.org/10.1016/s0040-1951(97)00050-4.
Gervilla, F., Proenza, J.A., Frei, R., González-Jiménez, J.M., Garrido, C.J., Melgarejo, J.C., et al., 2005. Distribution of platinum-group elements and Os isotopes in chromite ores from Mayarí–Baracoa ophiolitic belt (eastern Cuba). Contrib. Mineral. Petrol. 150, 589–607. http://dx.doi.org/10.1007/s00410-005-0039-2.
Ghasemi, H., Juteau, T., Bellon, H., Sabzehei, M., Whitechurch, H., Ricou, L.M., 2002. The mafic–ultramafic complex of Sikhoran (Central Iran): a polygenetic ophiolitic complex. Geosci. Front. 334, 431–438.
Ghosh, B., Morishita, T., Bhatta, K., 2013. Significance of chromian spinels from the mantle sequence of the Andaman Ophiolite, India: paleogeodynamic implications. Lithos 164–167, 86–96. http://dx.doi.org/10.1016/j.lithos.2012.08.004.
González-Jiménez, J.M., Proenza, J.A., Gervilla, F., Melgarejo, J.C., Blanco-Moreno, J.A., RuizSánchez, R., et al., 2011. High-Cr and high-Al chromitites from the Sagua de Tánamo district, Mayarí-Cristal ophiolitic massif (eastern Cuba): constraints on their origin from mineralogy and geochemistry of chromian spinel and platinum-group elements. Lithos 125 (1–2), 101–121. http://dx.doi.org/10.1016/j.lithos.2011.01.016.
Grammatikopoulos, T.A., Kapsiotis, A., Tsikouras, B., Hatzipanagiotou, K., Zaccarini, F., Garuti, G., 2011. Spinel composition, PGE geochemistry and mineralogy of the chromitites from the Vourinos ophiolite complex, Northwestern Greece. Can. Mineral. 49, 1571–1598.
Hickey, R.L., Frey, F.A., 1982. Geochemical characteristics of boninite series volcanics: implications for their source. Geochim. Cosmochim. Acta 46, 2099–2115. http://dx.doi.org/10.1016/0016-7037(82)90188-0.
Hillebrand, J., 1983. Chromite deposits in the province of Kerman. Iran. Ind. Miner. 35–43 (May 1983).
Irvine, T.N., 1967. Chromian spinel as a petrogenetic indicator: part 2. Petrologic applications. Can. J. Earth Sci. 4, 71–103. http://dx.doi.org/10.1139/e67-004.
Ishi, T., Robinson, P.T., Maekawa, H., Fiske, R., 1992. Petrological studies of peridotites from diapiric serpentinite seamounts in the Izu–Ogazawara–Mariana forearc, leg 125. In: Fryer, P., Pearce, J.A., Stocking, L.B., et al. (Eds.), Proceedings of the Ocean Drilling ProgramScientific Results 125. College Station, Texas, pp. 445–485.
Ishikawa, T., Nagaishi, K., Umino, S., 2002. Boninitic volcanism in the Oman ophiolite: implications for thermal condition during transition from spreading ridge to arc. Geology 30, 899–902.
Ishimaru, S., Arai, S., 2008. Nickel enrichment in mantle olivine beneath a volcanic front. Contrib. Mineral. Petrol. 156, 119–131.
Ismail, S.A., Mirza, T.M., Carr, P.F., 2010. Platinum-group elements geochemistry in podiform chromitites and associated peridotites of the Mawat ophiolite, northeastern Iraq. J. Asian Earth Sci. 37, 31–41. http://dx.doi.org/10.1016/j.jseaes.2009.07.005.
Jan, M.Q., Windley, B.F., 1990. Chromian spinel-silicate chemistry in ultrabasic rocks of the Jijal complex, Northwest Pakistan. J. Petrol. 31, 667–715.
Jannessary, M.R., Melcher, F., Lodziak, J., Meisel, T.C., 2012. Review of platinum-group element distribution and mineralogy in chromitite ores from southern Iran. Ore Geol. Rev. 48, 278–305. http://dx.doi.org/10.1016/j.oregeorev.2012.05.001.
Jenner, G.A., 1981. Geochemistry of high-Mg andesites from Cape Vogel, Papua New Guinea. Chem. Geol. 33, 307–332. http://dx.doi.org/10.1016/0009-2541(81)90106–6.
Johnson, K.T.M., Dick, H.J.B., Shimizu, N., 1990. Melting in the oceanic upper mantle: an ion microprobe study of diopsides in abyssal peridotites. J. Geophys. Res. Solid Earth 95, 2661–2678. http://dx.doi.org/10.1029/JB095iB03p02661.
Kamenetsky, V.S., Crawford, A.J., Meffre, S., 2001. Factors controlling chemistry of magmatic spinel: an empirical study of associated olivine, Cr-spinel and melt inclusions from primitive rocks. J. Petrol. 42, 655–671. http://dx.doi.org/10.1093/petrology/42.4.655.
Kamenetsky, V.S., Sobolev, A.V., Eggins, S.M., Crawford, A.J., Arculus, R.J., 2002. Olivineenriched melt inclusions in chromites from low-Ca boninites, Cape Vogel, Papua New Guinea: evidence for ultramafic primary magma, refractory mantle source and enriched components. Chem. Geol. 183, 287–303. http://dx.doi.org/10.1016/S0009-2541(01)00380–1.
Kapsiotis, A.N., 2014. Compositional signatures of SSZ-type peridotites from the northern Vourinos ultra-depleted upper mantle suite, NW Greece. Chem. Erde. Geochem. 74, 783–801. http://dx.doi.org/10.1016/j.chemer.2014.05.004.

Kapsiotis, A., Grammatikopoulos, T.A., Tsikouras, B., Hatzipanagiotou, K., Zaccarini, F., Garuti, G., 2009. Chromian spinel composition and Platinum-group element mineralogy of chromitites from the Milia area, Pindos ophiolite complex, Greece. Can. Mineral. 47, 1037–1056.

Kapsiotis, A., Grammatikopoulos, T., Tsikouras, B., Hatzipanagiotou, K., Zaccarini, F., Garuti, G., 2011. Mineralogy, composition and PGM of chromitites from Pefki, Pindos ophiolite complex (NW Greece): evidence for progressively elevated fAs conditions in the upper mantle sequence. Miner. Petrol. 101, 29–50.

Kojonen, K., Zaccarini, F., Garuti, G., 2003. Platinum-group elements and gold geochemistry and mineralogy in the Ray-Iz ophiolitic chromitites, Polar Urals. In: Eliopoulos, D.G., et al. (Eds.), Mineral Exploration and Sustainable Development. Millpress, Rotterdam, pp. 599–602.

Le Maitre, R.W., 2002. Igneous rocks – a classification and glossary of terms. Recommendations of the IUGS subcommission on the Systematics of Igneous Rocks. second ed. Cambridge University Press, Cambridge.

Le Roex, A.P., Dick, H.J.B., Gulen, L., Reid, A.M., Erlank, A.J., 1987. Local and regional heterogeneity in MORB from the mid-Atlantic ridge between 54.5°S and 51°S: evidence for geochemical enrichment. Geochim. Cosmochim. Acta 51, 541–555. http://dx.doi.org/10.1016/0016-7037(87)90068–8.

Leblanc, M., 1991. Platinum-group elements and gold in ophiolitic complexes: distribution and fractionation from mantle to oceanic floor. In: Peters, T. (Ed.), Ophiolite Genesis and Evolution of the Oceanic Lithosphere, Oman. Kluwer, Dordrecht, pp. 231–260.

Lemaire, M.M., Westphal, M., Gurevitch, E.L., Nazarov, K., Feinberg, H., Pozzi, J.P., 1997. How far between Iran and Eurasia was the Turan plate during Triassic–Jurassic times? Geol. Mijnb. 76, 73–82. http://dx.doi.org/10.1023/a:1003129028277.

Luguet, A., Lorand, J.-P., Seyler, M., 2003. Sulfide petrology and highly siderophile element geochemistry of abyssal peridotites: a coupled study of samples from the Kane Fracture Zone (45°W 23°20 N, MARK area, Atlantic Ocean). Geochim. Cosmochim. Acta 67, 1553–1570. http://dx.doi.org/10.1016/s0016-7037(02)01133-x.

Maurel, C., Maurel, P., 1982. Étude expérimentale de la distribution de l'aluminium entre bain silicaté basique et spinelle chromifère. Implications pétrogénétiques: teneur en chrome des spinelles. Bull. Mineral. 105, 197–202.

Maurel, C., 1984. Etude expérimentale de l´équilibre spinelle chromifère liquide silicaté basique. SFMC Meeting "Les spinelles", Lille (oral communication)..

McCall, G.J.H., 1985. Explanatory text of the Minab Quadrangle Map; 1:250,000; No. J13, Geological Survey of Iran, Tehran, 530p.

McCall, G.J.H., 1997. The geotectonic history of the Makran and adjacent areas of southern Iran. J. Asian Earth Sci. 15, 517–531. http://dx.doi.org/10.1016/S0743-9547(97)00032–9.

McDonald, A.M., Proenza, J.A., Zaccarini, F., Rudashevsky, N.S., Cabri, L.J., Stanley, C.J., Rudashevsky, V.N., Melgarejo, J.C., Lewis, J.F., Longo, F., Bakker, R.J., 2010. Garutiite, (Fe,Ni,Ir), a new hexagonal polymorph of native Ni from Loma Peguera, Dominican Republic. Eur. J. Mineral. 22, 293–304.

McDonough, W.F., Sun, S.S., 1995. The chemical composition of the Earth. Chem. Geol. 120, 223–253.

Melcher, F., Grum, W., Simon, G., Thalhammer, T.V., Stumpfl, E.F., 1997. Petrogenesis of the ophiolitic giant chromite deposits of Kempirsai, Kazakhstan: a study of solid and fluid inclusions in chromite. J. Petrol. 38, 1419–1458. http://dx.doi.org/10.1093/petroj/38.10.1419.

Moghadam, H.S., Stern, R.J., Rahgoshay, M., 2010. The Dehshir ophiolite (central Iran): Geochemical constraints on the origin and evolution of the Inner Zagros ophiolite belt. Geol. Soc. Am. Bull. 122, 1516–1547.

Najafzadeh, A.R., Ahmadipour, H., 2014a. Using platinum-group elements and Au geochemistry to constrain the genesis of podiform chromitites and associated peridotites from the Soghan mafic–ultramafic complex, Kerman, Southeastern Iran. Ore Geol. Rev. 60, 60–75. http://dx.doi.org/10.1016/j.oregeorev.2013.12.014.

Najafzadeh, A.R., Ahmadipour, H., 2014b. Platinum-group elements (PGE) and chromian spinel geochemistry in the peridotites from the Abdasht ultramafic complex, Kerman, Southeastern Iran. Olum-i-Zamin. 91, 173–186 (In Persian).

Najafzadeh, A.R., Arvin, M., Pan, Y., Ahmadipour, H., 2008. Podiform chromitites in the Sorkhband ultramafic complex, Southern Iran: evidence for ophiolitic chromitite. J. Sci. Islam. Repub. Iran 19, 49–65.

Naldrett, A.J., Duke, J.M., 1980. Platinum metals in magmatic sulfide ores. Science 208, 1417–1424.

Ohara, Y., 2006. Mantle process beneath Philippine Sea back-arc spreading ridges: a synthesis of peridotite petrology and tectonics. Island Arc 15, 119–129. http://dx.doi.org/10.1111/j.1440-1738.2006.00515.x.

Okamura, H., Arai, S., Kim, Y.-U., 2006. Petrology of forearc peridotite from the Hahajima Seamount, the Izu-Bonin arc, with special reference to chemical characteristics of chromian spinel. Min. Mag. 70, 15–26.

Orberger, B., Lorand, J.P., Girardeau, J., Mercier, J.C.C., Pitragool, S., 1995. Petrogenesis of ultramafic rocks and associated chromitites in the Nan Uttaradit ophiolite, Northern Thailand. Lithos 35, 153–182. http://dx.doi.org/10.1016/0024-4937(94)00041-y.

Pagé, P., Barnes, S.-J., 2009. Using trace elements in chromites to constrain the origin of podiform chromitites in the Thetford Mines Ophiolite, Québec, Canada. Econ. Geol. 104, 997–1018.

Parkinson, I.J., Pearce, J.A., 1998. Peridotites from the Izu–Bunin–Mariana forearc (ODP Leg 125): evidence for mantle melting and melt–mantle interaction in a supra-subduction zone setting. J. Petrol. 39, 1577–1618.

Pašava, J., Vymazalová, A., Petersen, S., Herzig, P., 2004. PGE distribution in massive sulfides from the PACMANUS hydrothermal field, eastern Manus basin, Papua New Guinea: implications for PGE enrichment in some ancient volcanogenic massive sulfide deposits. Mineral. Deposita 39, 784–792. http://dx.doi.org/10.1007/s00126-004-0442-z.

Pearce, J.A., Barker, P.F., Edwards, S.J., Parkinson, I.J., Leat, P.T., 2000. Geochemistry and tectonic significance of peridotites from the South Sandwich arc-basin system, South Atlantic. Contrib. Mineral. Petrol. 139, 36–53.

Peighambari, S., Ahmadipour, H., Stosch, H.-G., Daliran, F., 2011. Evidence for multi-stage mantle metasomatism at the Dehsheikh peridotite massif and chromite deposits of the Orzuieh coloured mélange belt, southeastern Iran. Ore Geol. Rev. 39, 245–264. http://dx.doi.org/10.1016/j.oregeorev.2011.03.004.

Peighambari, S., Uysal, I., Stosch, H.-G., Ahmadipour, H., Heidarian, H., 2016. Genesis and tectonic setting of ophiolitic chromitites from the Dehsheikh ultramafic complex (Kerman, southeastern Iran): Inferences from platinum-group elements and chromite compositions. Ore Geology Reviews. 74, 39–51.

Presnall, D.C., Hoover, J.D., 1987. High pressure phase equilibrium constraints on the origin of mid-ocean ridge basalts. Geochem. Soc. Spec. Publ. 1, 75–89.

Proenza, J.A., Zaccarini, F., Lewis, J.F., Longo, F., Garuti, G., 2007. Chromian spinel composition and the platinum-group minerals of the PGE-rich Loma Peguera chromitites, Loma Caribe peridotite, Dominican Republic. Can. Mineral. 45, 31–48. http://dx.doi.org/10.2113/gscanmin.45.3.631.

Rajabzadeh, M.A., Nazari Dehkordi, T., Caran, Ş., 2013. Mineralogy, geochemistry and geotectonic significance of mantle peridotites with high-Cr chromitites in the Neyriz ophiolite from the outer Zagros ophiolite belts, Iran. J. Afr. Earth Sci. 78, 1–15. http://dx.doi.org/10.1007/s00710-012-0265-z.

Ravikant, V., Pal, T., Das, D., 2004. Chromites from the Nidar ophiolite and Karzok complex, Transhimalaya, eastern Ladakh: their magmatic evolution. J. Asian Earth Sci. 24, 177–184. http://dx.doi.org/10.1016/j.jseaes.2003.10.005.

Robinson, P.T., Melson, W.G., O'Hearn, T., Schmincke, H.-U., 1983. Volcanic glass compositions of the Troodos ophiolite, Cyprus. Geology 11, 400–404. http://dx.doi.org/10.1130/0091-7613(1983)11<400:vgcott>2.0.co;2.

Rollinson, H., 2008. The geochemistry of mantle chromitites from the northern part of the Oman ophiolite: inferred parental melt compositions. Contrib. Mineral. Petrol. 156, 273–288. http://dx.doi.org/10.1007/s00410-008-0284-2.

Sabzehei, M., 1974. Les melange ophiolitiques de la region d'Esfandegheh, these d'etate. Universite scientifique et medicale de Grenobe, France (306 pp.).

Schmidt, H.L., 1974. Iran. Rohstoffwirtschaftliche Länderberichte, Teil V. Bundesanstalt für Bodenforschung, p. 89.

Schwab, B.E., Johnston, A.D., 2001. Melting systematic of modally variable, compositionally intermediate peridotites and the effects of mineral fertility. J. Petrol. 42, 1789–1811.

Shafaii Moghadam, H., Stern, R.J., 2011. Geodynamic evolution of Upper Cretaceous Zagros ophiolites: formation of oceanic lithosphere above a nascent subduction zone. Geol. Mag. 148, 762–801. http://dx.doi.org/10.1017/S0016756811000410.

Shafaii Moghadam, H., Mosaddegh, H., Santosh, M., 2013. Geochemistry and petrogenesis of the Late Cretaceous Haji-Abad ophiolite (Outer Zagros Ophiolite Belt, Iran): implications for geodynamics of the Bitlis–Zagros suture zone. Geol. J. 48, 579–602. http://dx.doi.org/10.1002/gj.2458.

Shen-Su, S., 1982. Chemical composition and origin of the earth's primitive mantle. Geochim. Cosmochim. Acta 46, 179–192. http://dx.doi.org/10.1016/0016-7037(82)90245-9.

Shibata, T., Thompson, G., Frey, F.A., 1979. Tholeiitic and alkali basalts from the mid Atlantic ridge at 43°N. Contrib. Mineral. Petrol. 70, 127–141. http://dx.doi.org/10.1007/bf00374441.

Su, B.-X., Qin, K.-Z., Sakyi, P.A., Li, X.-H., Yang, Y.-H., Sun, H., et al., 2011. U–Pb ages and Hf–O isotopes of zircons from Late Paleozoic mafic–ultramafic units in the southern Central Asian Orogenic Belt: Tectonic implications and evidence for an Early-Permian mantle plume. Gondwana Res. 20, 516–531. http://dx.doi.org/10.1016/j.gr.2010.11.015.

Tamura, A., Arai, S., 2006. Harzburgite–dunite–orthopyroxenite suite as a record of supra-subduction zone setting for the Oman ophiolite mantle. Lithos 90, 43–56. http://dx.doi.org/10.1016/j.lithos.2005.12.012.

Thanh, N.X., Hai, T.T., Hoang, N., Lan, V.Q., Kwon, S., Itaya, T., et al., 2014. Backarc mafic–ultramafic magmatism in Northeastern Vietnam and its regional tectonic significance. J. Asian Earth Sci. 90, 45–60. http://dx.doi.org/10.1016/j.jseaes.2014.04.001.

Tsoupas, G., Economou-Eliopoulos, M., 2008. High PGE contents and extremely abundant PGE-minerals hosted in chromitites from the Veria ophiolite complex, northern Greece. Ore Geol. Rev. 33, 3–19. http://dx.doi.org/10.1016/j.oregeorev.2006.10.008.

Uysal, I., Tarkian, M., Sadiklar, M.B., Şen, C., 2007. Platinum-group-element geochemistry and mineralogy of ophiolitic chromitites from Kop Mountain, Northeastern Turkey. Can. Mineral. 45, 355–377. http://dx.doi.org/10.2113/gscanmin.45.2.355.

Uysal, I., Tarkian, M., Sad ı klar, B., Zaccarini, F., Meisel, T., Garuti, G., Heidrich, S., 2009. Petrology of Al- and Cr-rich ophiolitic chromitites from the Muğla, SW Turkey: implications from composition of chromite, solid inclusions of platinum-group mineral, silicate, and base-metal mineral, and Os-isotope geochemistry. Contrib. Mineral. Petrol. 158 (5), 659–674. http://dx.doi.org/10.1007/s00410-009-0402-9.

Walker, D.A., Cameron, W.E., 1983. Boninite primary magmas: evidence from the Cape Vogel Peninsula, PNG. Contrib. Mineral. Petrol. 83, 150–158. http://dx.doi.org/10.1007/bf00373088.

Wasylenki, L.E., Baker, M.B., Kent, A.J.R., Stolper, E.M., 2003. Near-solidus melting of the shallow upper mantle: partial melting experiments on depleted peridotite. J. Petrol. 44, 1163–1191. http://dx.doi.org/10.1093/petrology/44.7.1163.

Wensink, H., 1981. Le contact Gondwana-Eurasie en Iran d'apres les recherches paleomagnetiques. Bull. Soc. geol. Fr. Ser. 7 XXIII, 547–552. http://dx.doi.org/10.2113/gssgfbull.S7-XXIII.6.547.

Zhou, M.-F., Bai, W.-J., 1992. Chromite deposits in China and their origin. Mineral. Deposita 27, 192–199.

Zhou, M.-F., Bai, W.-J., 1994. Formation of podiform chromitites by melt/rock interaction in the upper mantle. Mineral. Deposita 29, 98–101.

Zhou, M.F., Robinson, P.T., Malpas, J., Li, Z., 1996. Podifrom chromitites in the Luobusa ophiolite (southern Tibet): implications for melt–rock interaction and chromite segregation in the upper mantle. J. Petrol. 37, 3–21. http://dx.doi.org/10.1093/petrology/37.1.3.

Zhou, M.-F., Sun, M., Keays, R.R., Kerrich, R.W., 1998. Controls on Platinum-group elemental distributions of podiform chromitites: a case study of high-Cr and high-Al chromitites from Chinese orogenic belts. Geochim. Cosmochim. Acta 62, 677–688. http://dx.doi.org/10.1016/s0016-7037(97)00382-7.

Zhou, M.-F., Robinson, P.T., Malpas, J., Edwards, S.J., Qi, L., 2005. REE and PGE geochemical constraints on the formation of dunites in the Luobusa ophiolite, Southern Tibet. J. Petrol. 46, 615–639. http://dx.doi.org/10.1093/petrology/egh091.